Laser-Driven High-Energy-Density Plasmas and Their Diagnostics

Proton radiograph

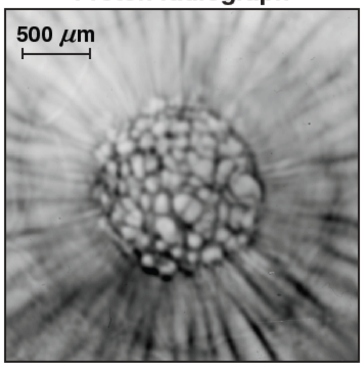

$t = t_0 + 2.6$ ns

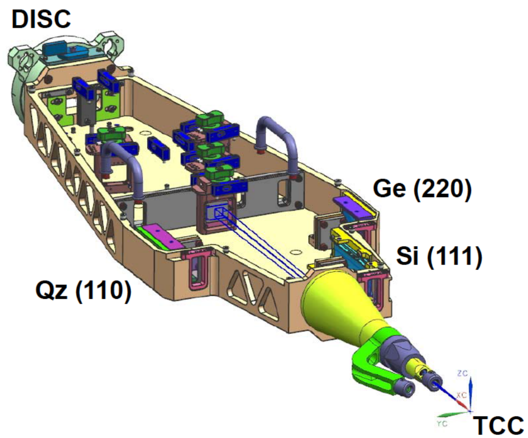

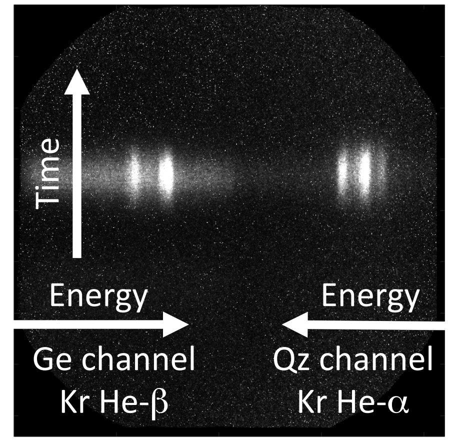

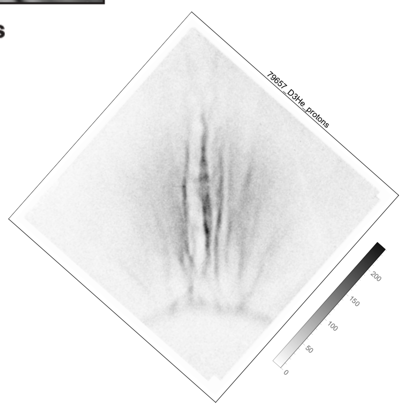

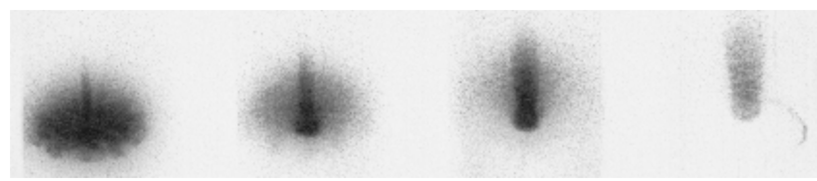

Lan Gao
Princeton Plasma Physics Laboratory
Princeton University

PPPL Graduate Summer School
August 17, 2018

Outline

- Introduction
  - High energy density (HED) physics
  - Inertial confinement fusion
  - Laser-driven HED systems
  - Diagnostic requirement
- Basic diagnostic building blocks
  - Electromagnetic field
  - Particles
  - X rays
    - Pinhole imaging
    - Streak cameras
    - Framing cameras
  - Plasma conditions

High energy density (HED) physics concerns the study of matter at high densities and extreme temperatures*

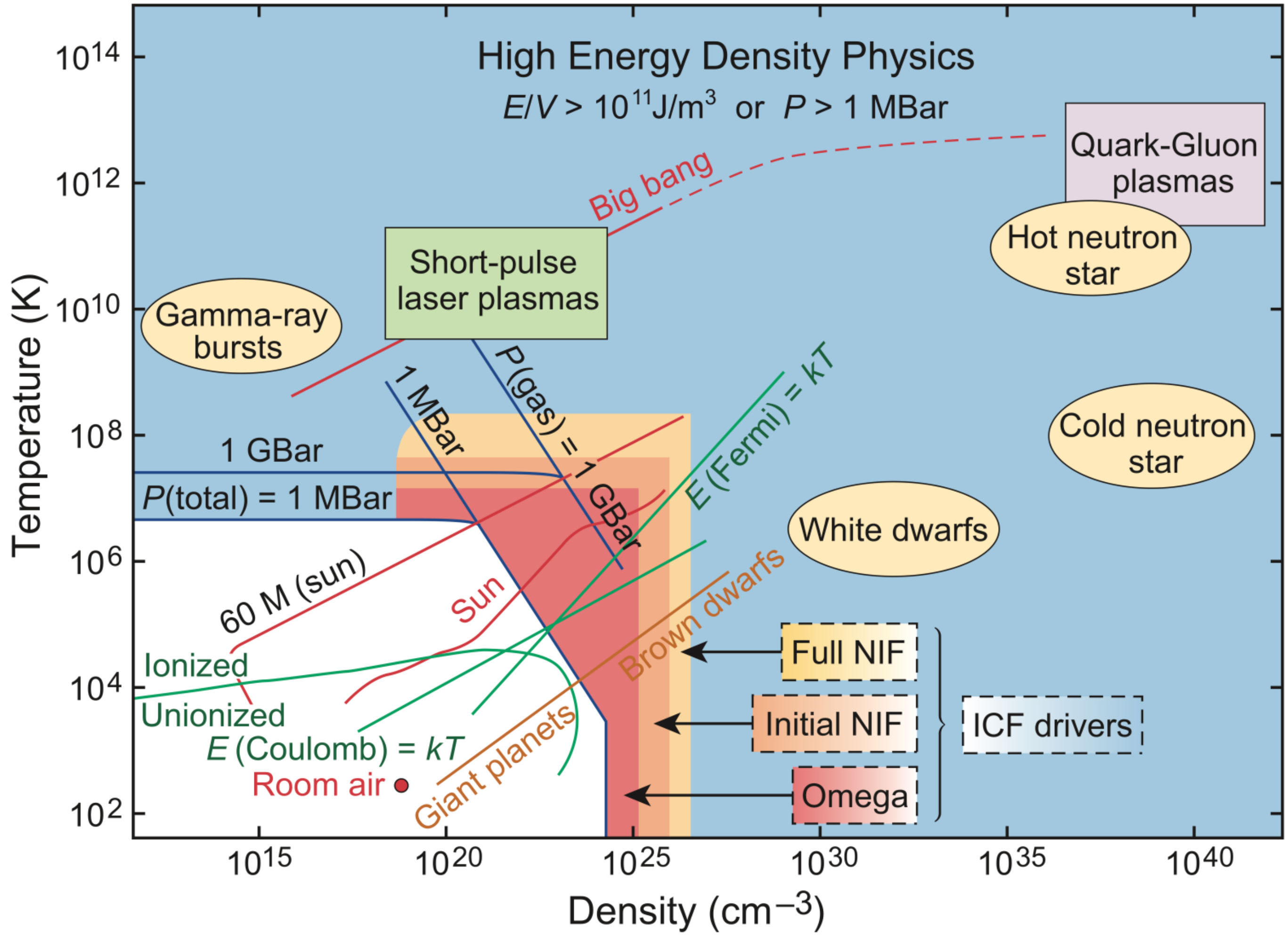

* *Frontiers in high energy density physics : The X-games of contemporary science.* (The National Academies Press, Washington, DC, 2003).

Laboratory for laser energetics (LLE) at University of Rochester operates two of the world's large lasers for HED physics research

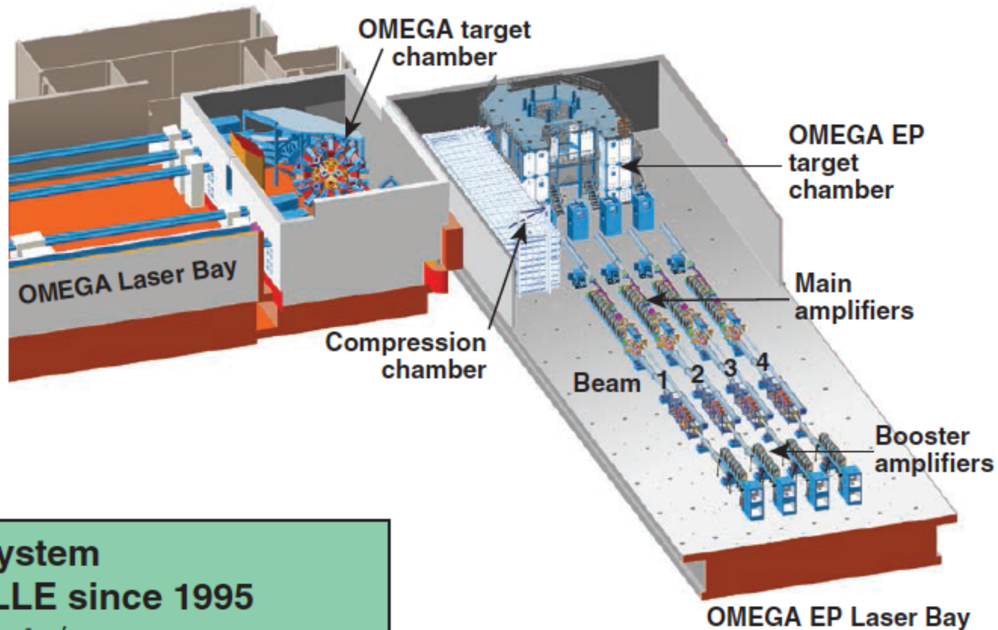

OMEGA Laser System

- Operating at LLE since 1995
- Up to 1500 shots/year
- Fully instrumented
- 60 beams
- >30-kJ UV on target
- 1% to 2% irradiation nonuniformity
- Flexible pulse shaping
- Short shot cycle (1 h)

More than half of OMEGA's shots are for external users.

OMEGA EP Laser System

- Completed 25 April 2008
- Four NIF-like beamlines; 6.5-kJ UV (10 ns)
- Two beams can be high-energy petawatt
  - 2.6-kJ IR in 10 ps
  - can propagate to the OMEGA or OMEGA EP target chamber

The National Ignition Facility (NIF) at LLNL aims at demonstrating fusion ignition

- The NIF is a 1.8-MJ laser system (60× OMEGA's energy); NIF is a $3.5 billion facility completed in 2009
- The NIF is performing experiments with the goal of achieving ignition

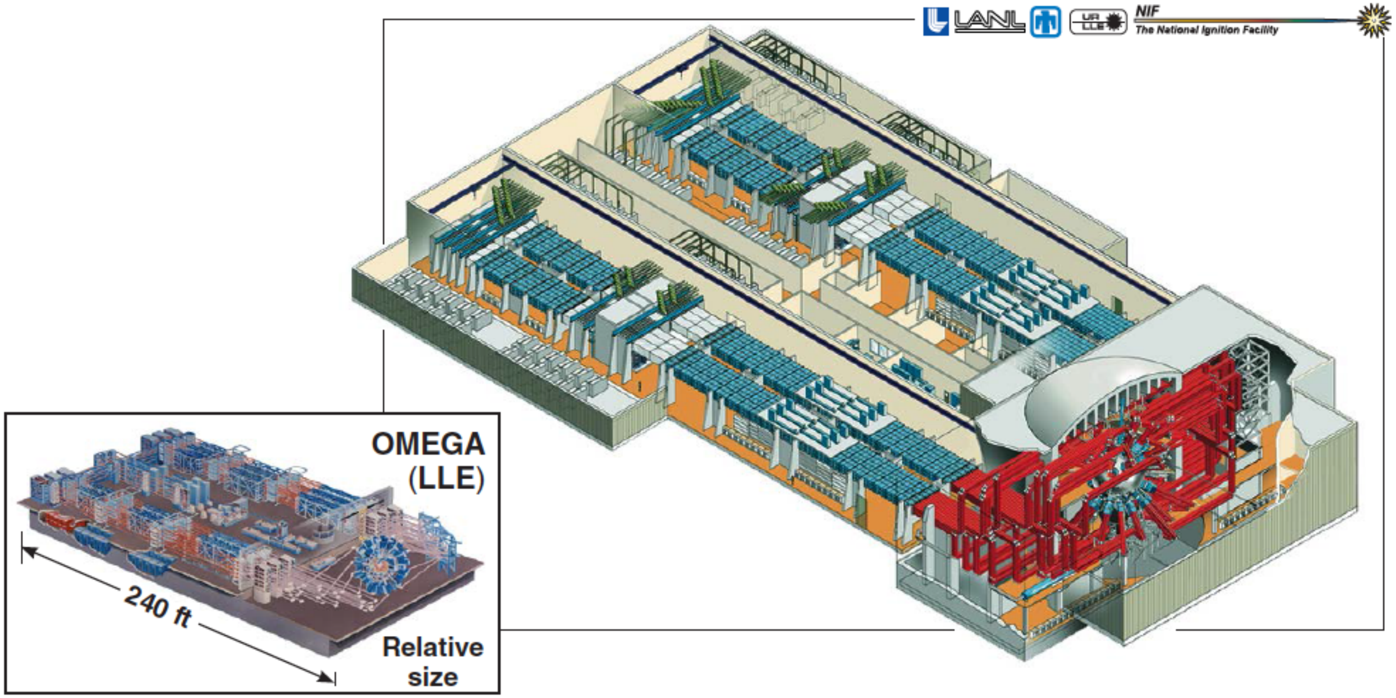

The achievement of ignition—a national "grand challenge"—on the NIF will change the fusion landscape.

Ablation is used to generate the extreme pressures required to compress a fusion capsule to ignition

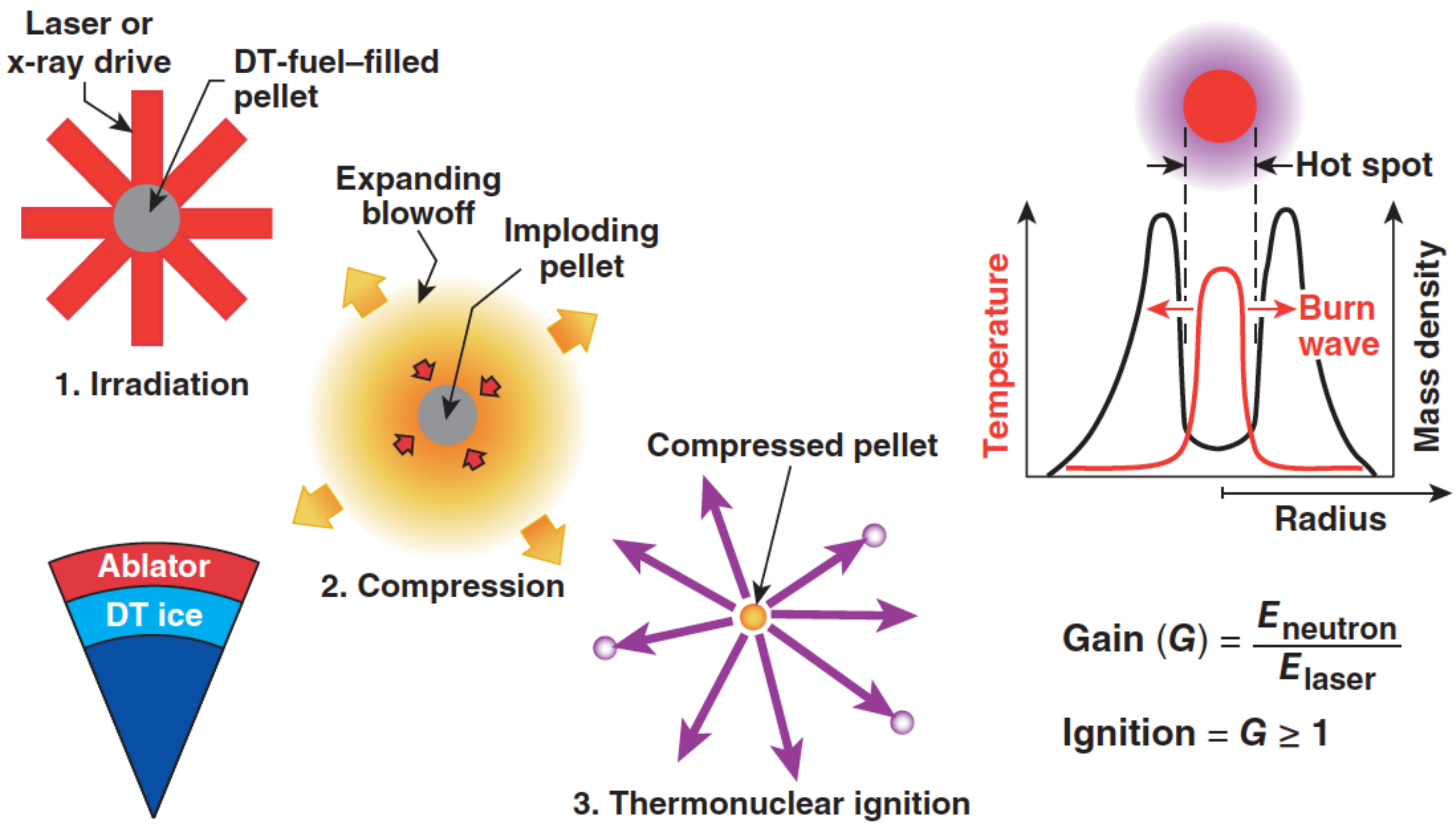

$$\text{Gain } (G) = \frac{E_{\text{neutron}}}{E_{\text{laser}}}$$

$$\text{Ignition} = G \geq 1$$

"Hot-spot" ignition requires the core temperature to be at least 5 keV and the core fuel areal density to exceed ~300 mg/cm^2.

Both direct and indirect (x-ray) drive are being used to implode the inertial confinement fusion capsules

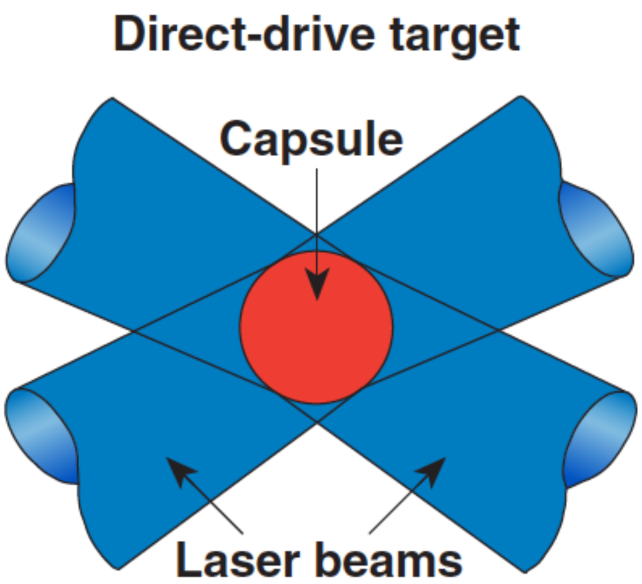

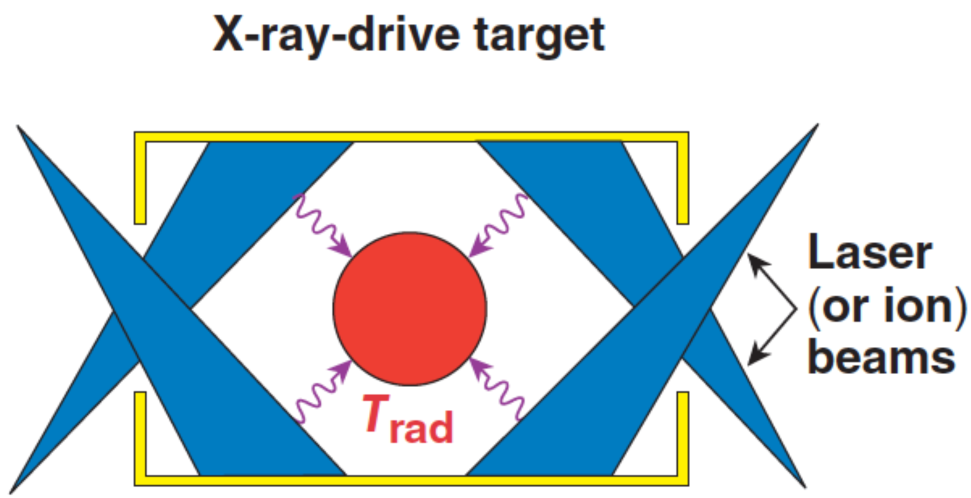

Hohlraum using
a cylindrical high-Z case
T_{rad} is the x-ray temperature

Key physics issues

- Energy coupling
- Drive uniformity
- Hydrodynamic instabilities
- Compressibility

Intense lasers create HED conditions in the laboratory through ablation

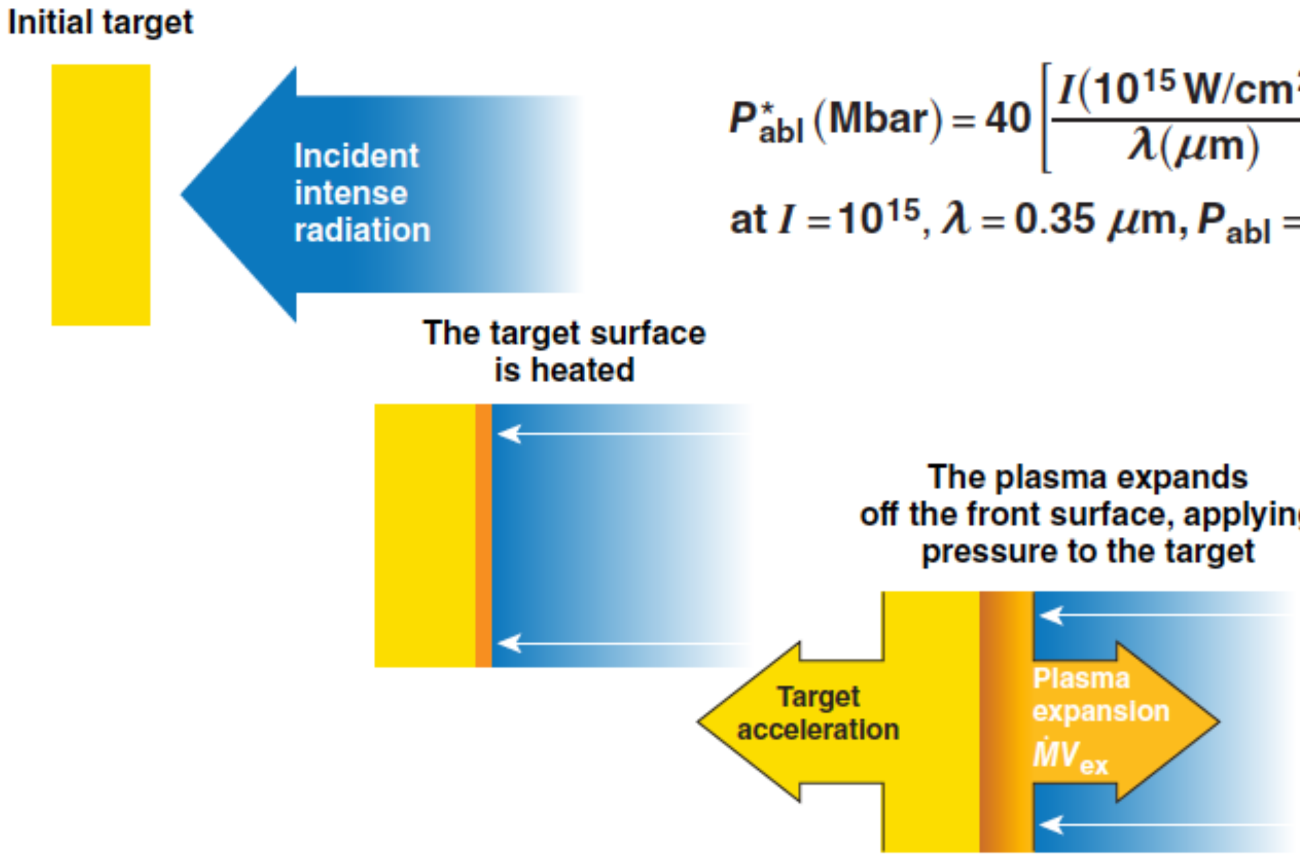

$$P^{*}_{abl}\,(\mathrm{Mbar}) = 40\left[\frac{I(10^{15}\,\mathrm{W/cm^2})}{\lambda(\mu\mathrm{m})}\right]^{2/3}$$

at $I = 10^{15}$, $\lambda = 0.35\ \mu$m, $P_{abl} = 80$ Mbar

E22082

*J. D. Lindl, *Inertial Confinement Fusion: The Quest for Ignition and Energy Gain Using Indirect Drive* (Springer-Verlag, New York, 1998).

If you look at the OMEGA target chamber

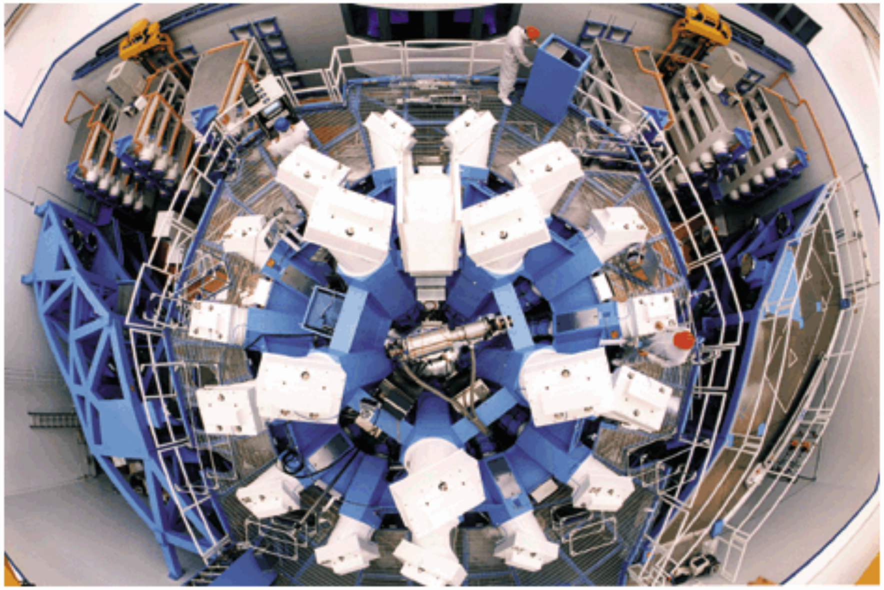

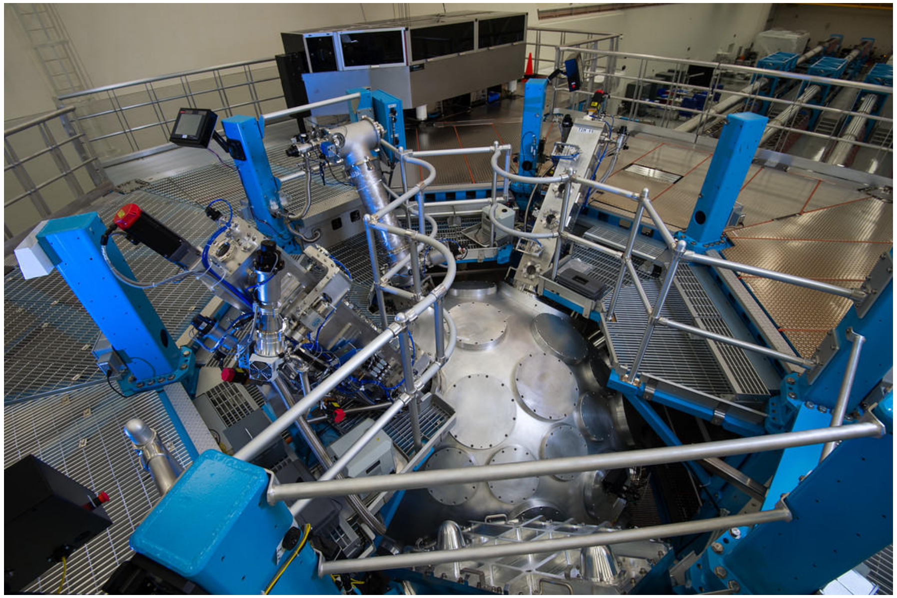

OMEGA **OMEGA EP**

If you look at the OMEGA target chamber

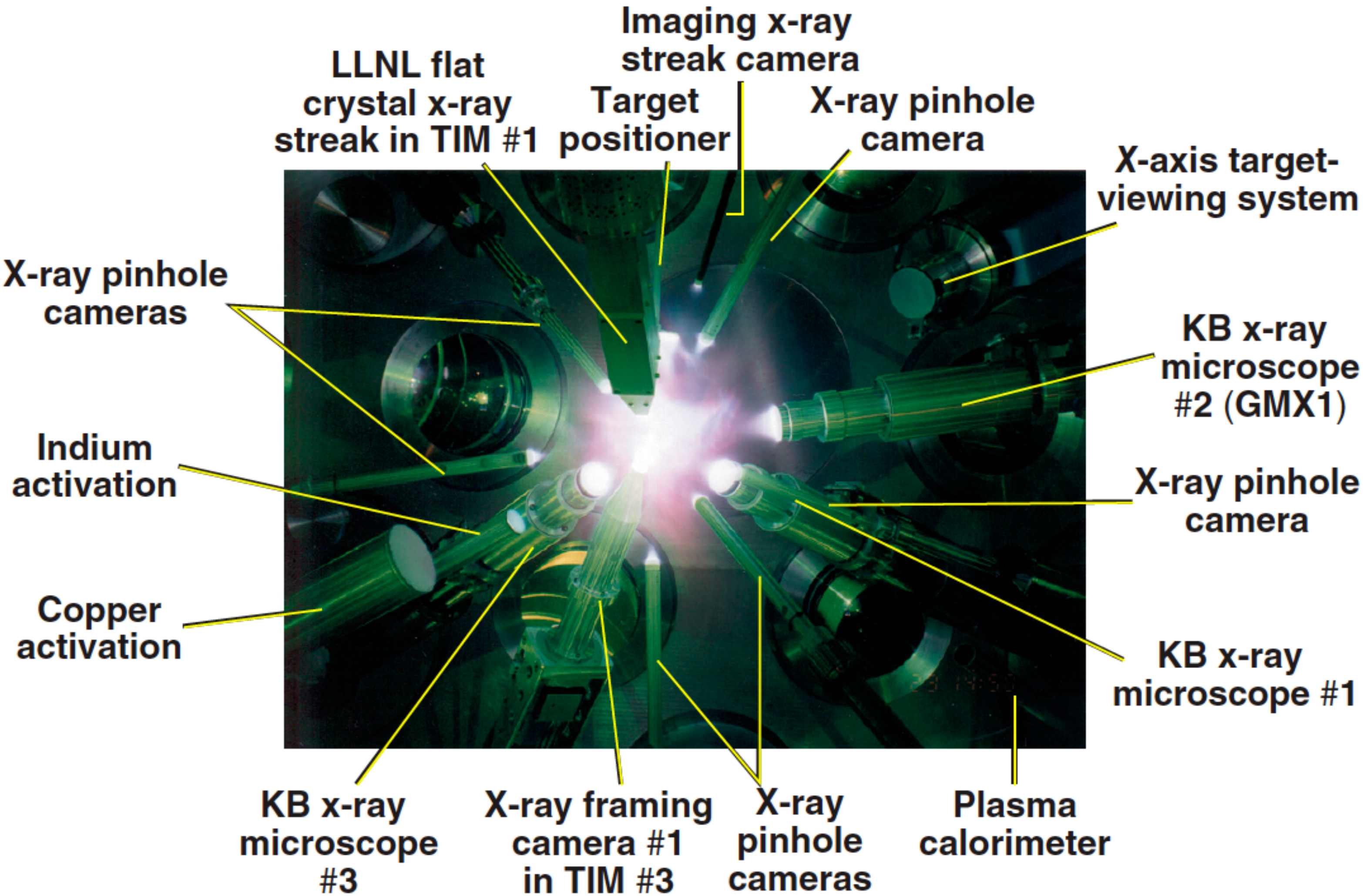

The NIF target chamber

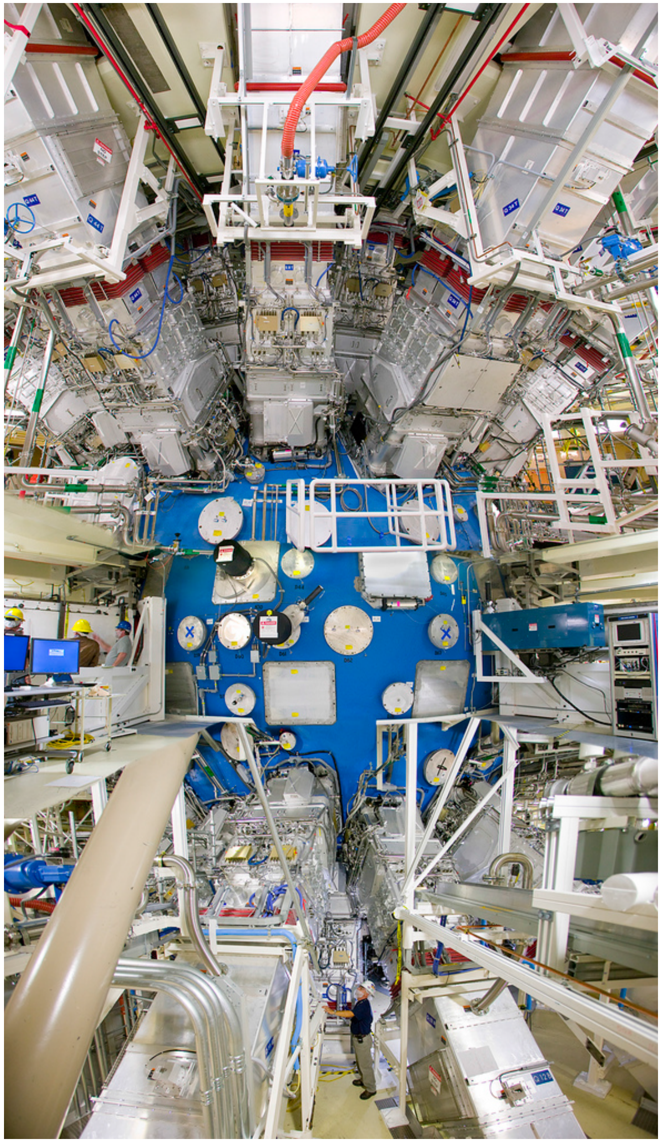

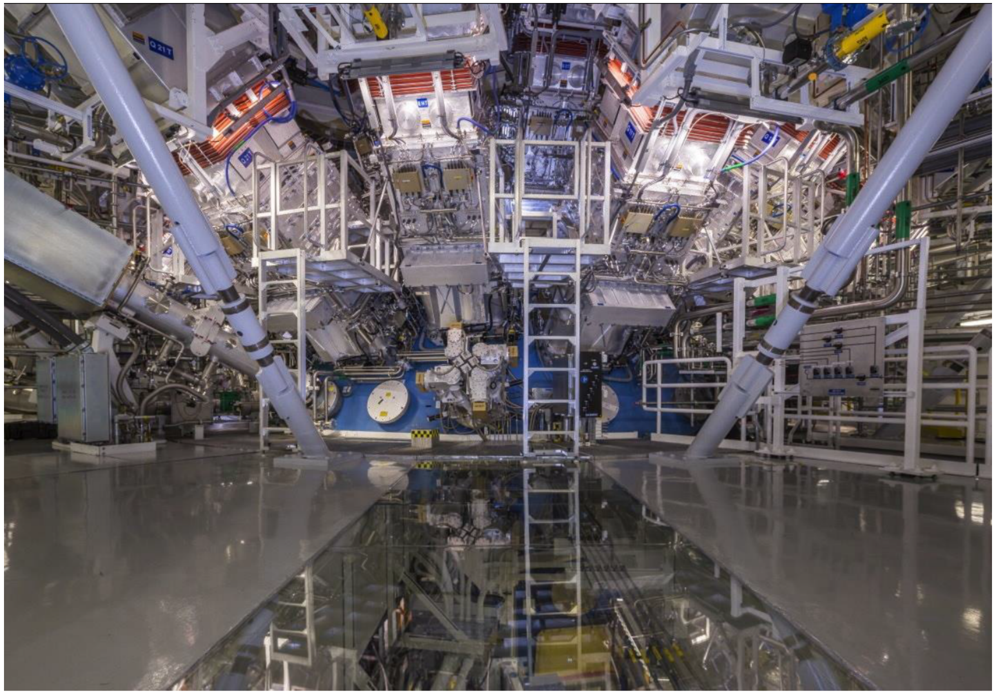

The NIF target chamber

Courtesy of Scott Chambliss, Paramount Pictures and Bad Robot Productions.

High-energy-density-physics (HEDP) systems are diagnosed by optical, x-ray, particle and nuclear means

- HEDP systems generate some or all of
  - Visible light
  - UV and x-ray photons
  - Charged particles
  - Neutrons
  - Strong fields
- A comprehensive diagnostic suite makes it possible to learn a great deal about the systems: field strength and their impact, plasma parameters (n_e, n_i, T_e, v), particles, instabilities, yield, etc…
- Diagnosing HED systems require very high temporal (sub-ns, ps) and spatial (~10 μm) resolution

Diagnostic performance is determined by the resolution and signal-to-noise levels

- Spatial, temporal, or energy resolution determines the diagnostic properties
- The resolution depends on the design and on the signal-to-noise (background) ratio
- The signal level depends on
  - Source brightness
  - Solid angle of the detector $\Delta\Omega = A_{det}/4\pi D^2$, where A is the effective diagnostic area, and D is the distance from the source to the diagnostic
- The noise (background) level is determined by design and intrinsic noise level (e.g., photon statistics)
- For example, when low number of particles (N) are detected, the uncertainty scales as sqrt(N)/N

Outline

- Basic diagnostic building blocks
  - Electromagnetic field
    - Proton radiography
  - Particles
    - RCF stack / Proton activation pack / Electron spectrometer / Thomson parabola
  - X rays
    - Pinhole camera (time integrated) / 1-D streak camera / 2-D framing camera
  - Plasma conditions
    - High-resolution x-ray spectroscopy / Thomson scattering / Neutrons / x-ray radiography

Outline

- Basic diagnostic building blocks
  - Electromagnetic field
    - Proton radiography
  - Particles
    - RCF stack / Proton activation pack / Electron spectrometer / Thomson parabola
  - X rays
    - Pinhole camera (time integrated) / 1-D streak camera / 2-D framing camera
  - Plasma conditions
    - High-resolution x-ray spectroscopy / Thomson scattering / Neutrons / x-ray radiography

Target Normal Sheath Acceleration (TNSA)* generates MeV proton beams in intense (>10^{18} W/cm^2) laser-solid interactions

- Hot electrons escape from the rear side of the target
- An electrostatic field is built up, with a field gradient of the order of MeV/μm
- Protons are accelerated to tens of MeV

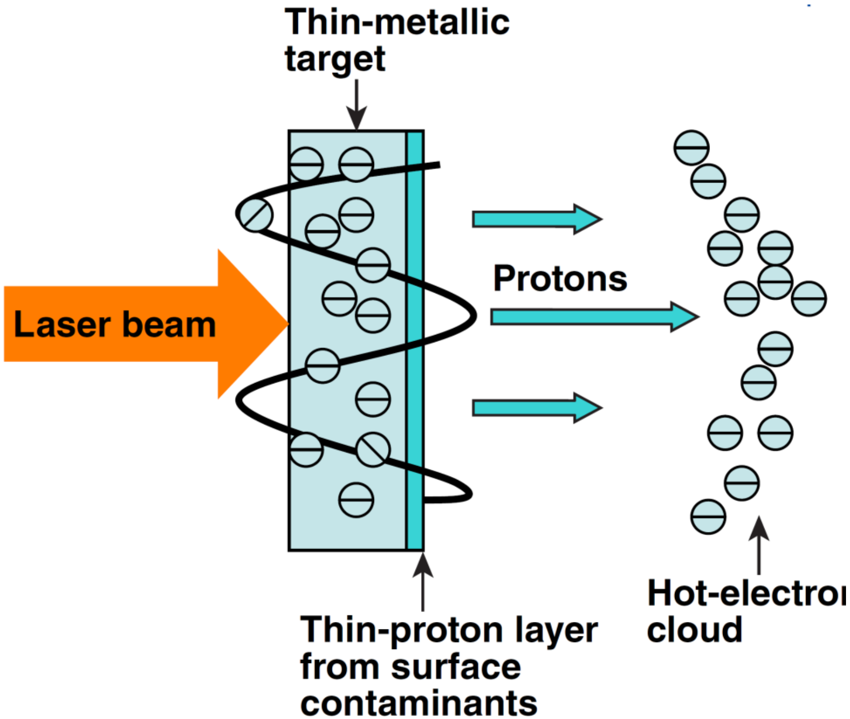

Laser-driven protons are ultra bright, extremely collimated, and have high peak energy (58 MeV) and short burst duration (picosecond scale).

---

*S. C. Wilks *et al.*, Phys. Plasma 8, 542 (2001)

The virtual proton source is much smaller than the laser spot*

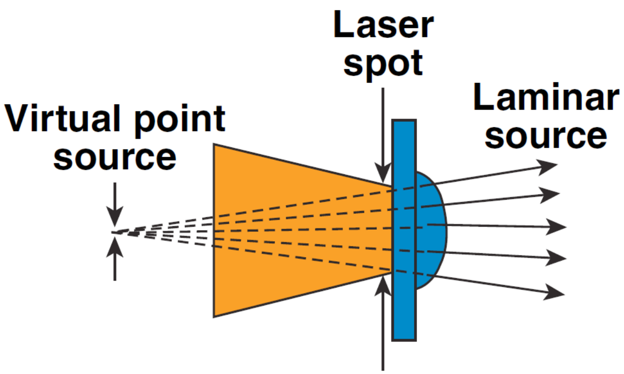

Virtual source size: 4±2 μm

Very high spatial resolution!

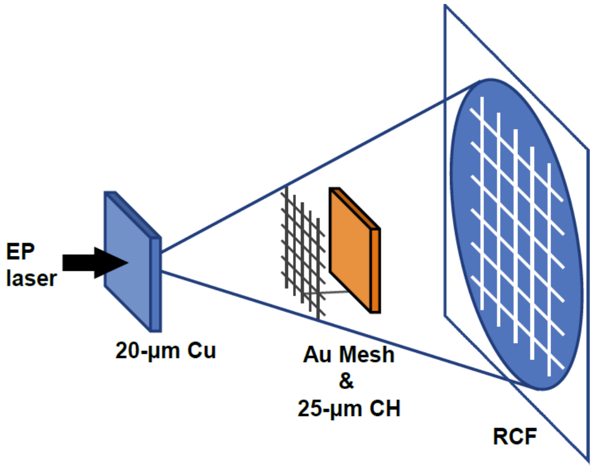

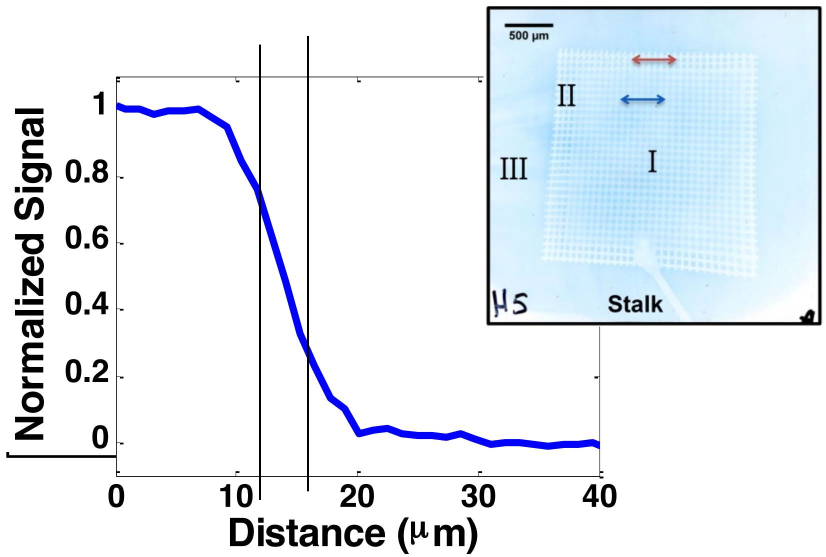

~ 8 µm for 15 MeV protons

Time-of-flight dispersion and a filtered stack detector produces a multiframe imaging capability

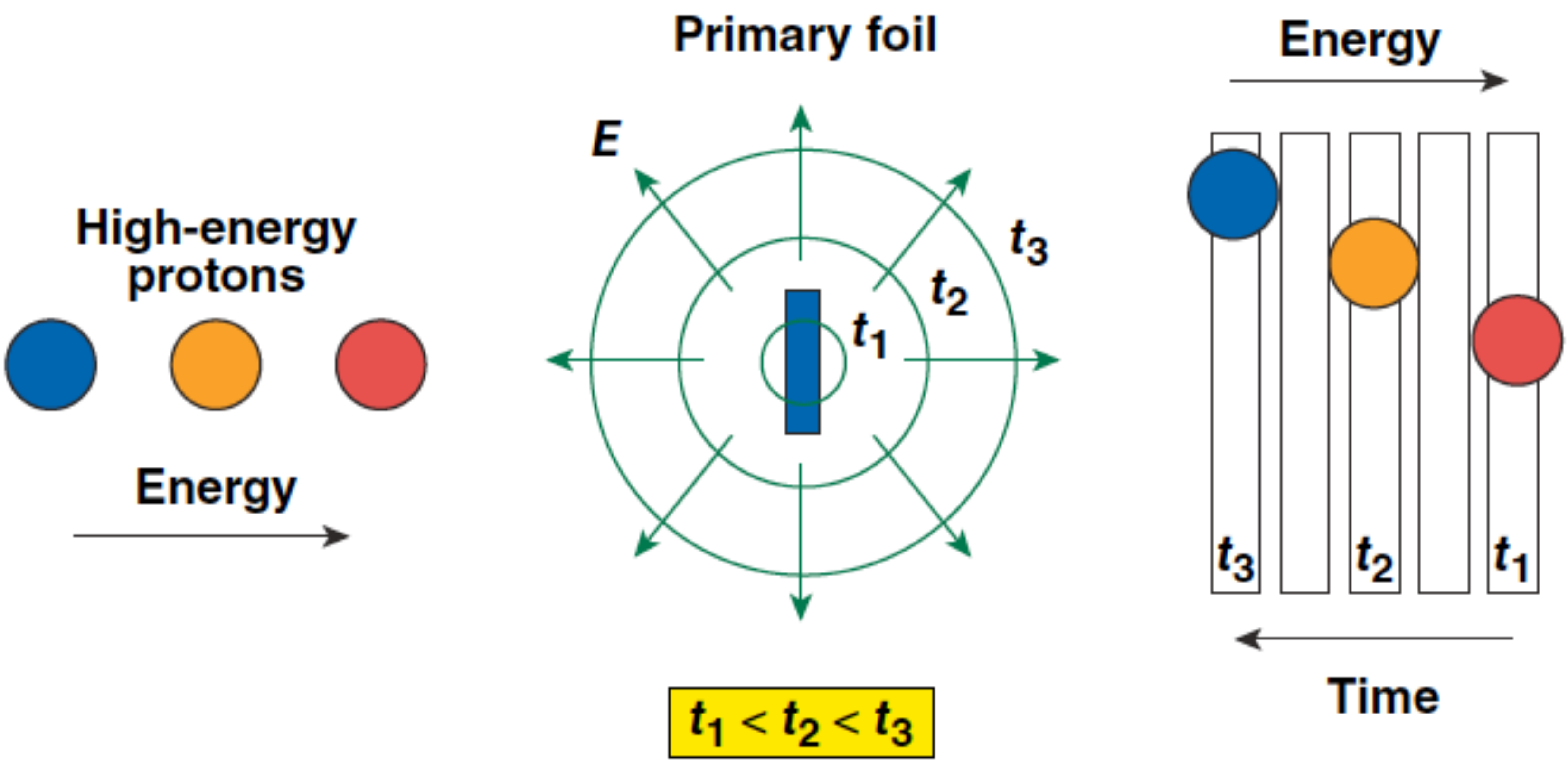

Ultrafast laser-driven proton radiography is developed on OMEGA EP

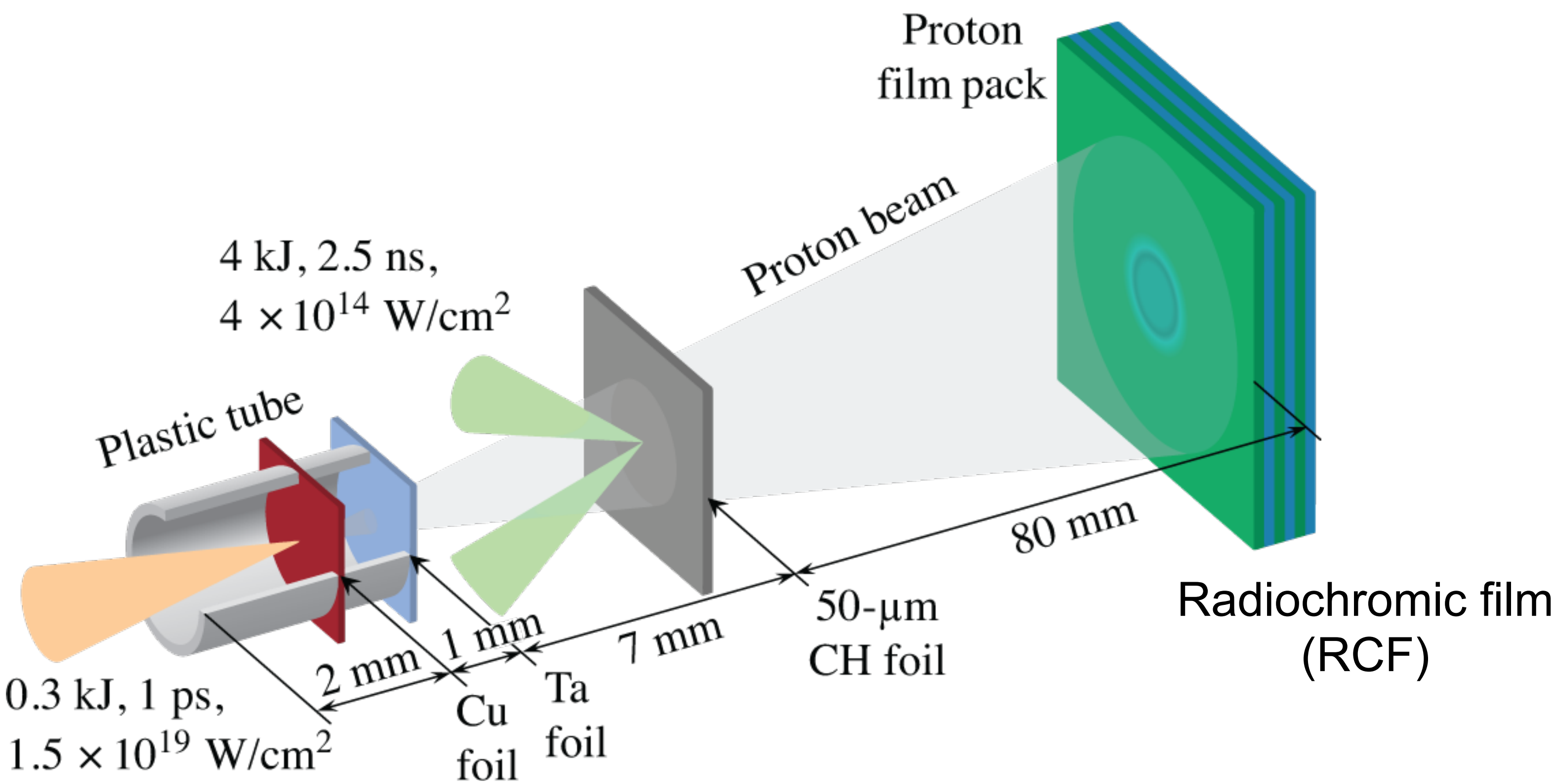

The laser-driven target is subjected to the Rayleigh-Taylor (RT) instability

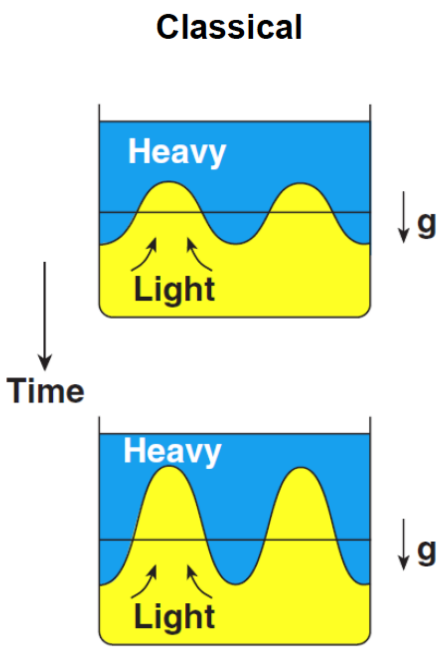

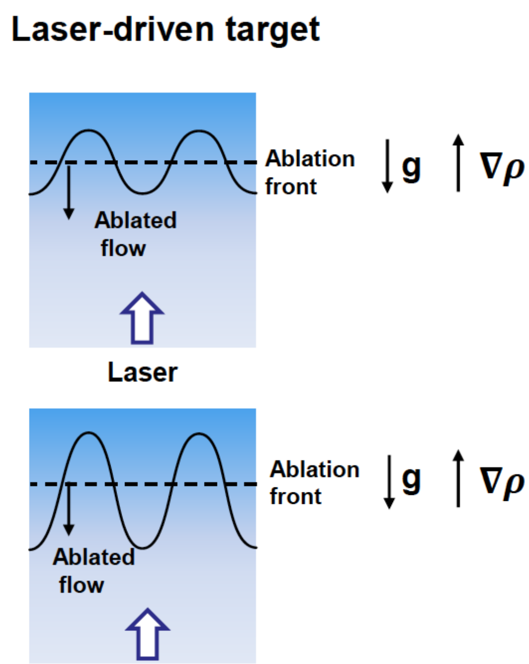

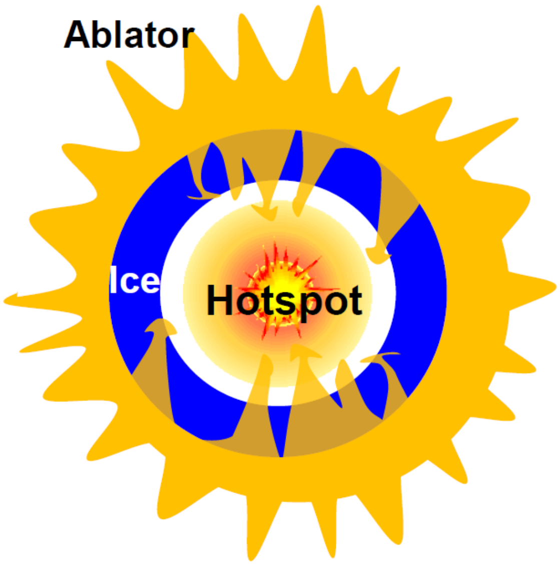

The RT instability has linear and nonlinear stages*

- Linear regime (classical)**:

$$\eta = \eta_0 e^{\gamma t}$$

$$\gamma = \sqrt{AKg}, \quad A = \frac{\rho_h - \rho_l}{\rho_h + \rho_l}$$

- Linear regime (ablative)**:

$$\gamma = \alpha\sqrt{\frac{Kg}{1+\epsilon KL}} - \beta K V_a$$

- Nonlinear regime***: $\eta \geq 0.1\lambda$

Slower growth

Bubbles and spikes

Bubble competition and merger

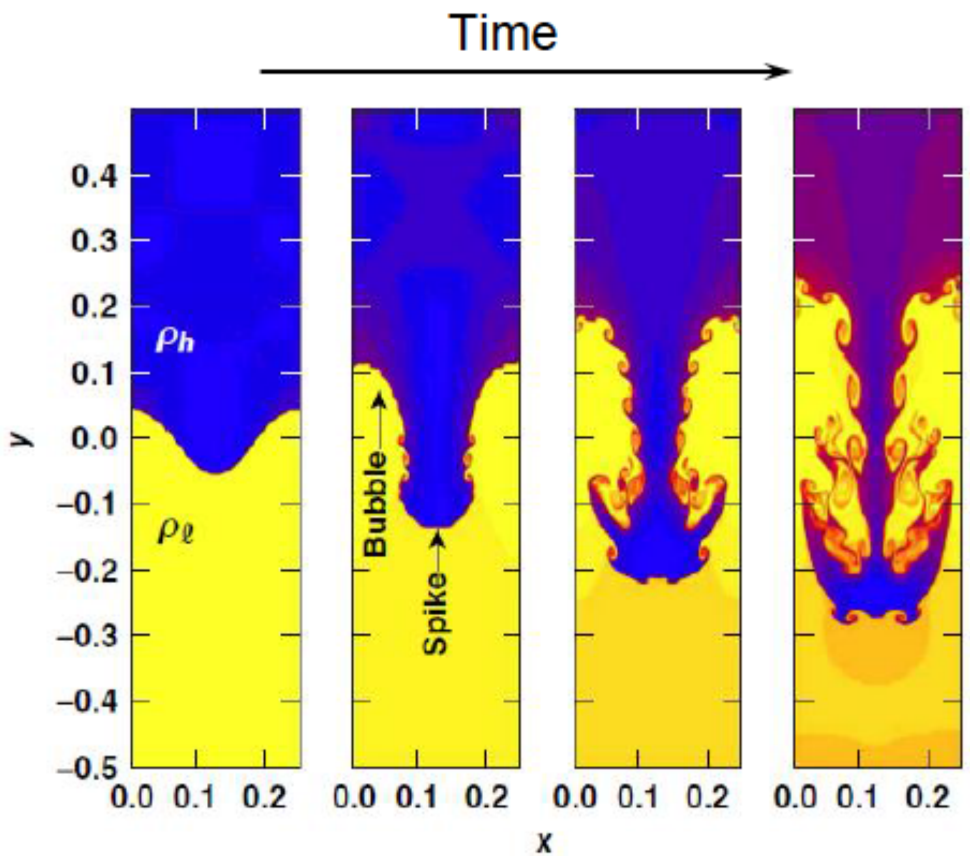

*Shengtai Li and Hui Li. "Parallel AMR Code for Compressible MHD or HD Equations". Los Alamos National Laboratory (2006).

**J. D. Kilkenny et al., Phys. Plasmas 1, 1379 (1994).

*** R. Betti and J. Sanz, Phy. Rev. Lett. 97, 205002 (2006).

Magnetic fields are generated by the Biermann battery mechanism

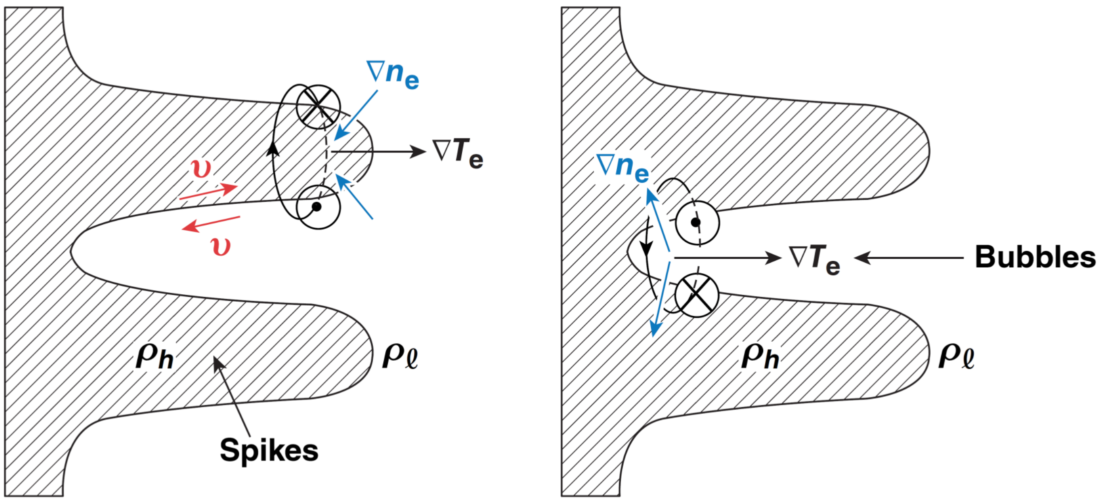

- **Biermann battery:**

$$\mathbf{E} = -\frac{\nabla P_e}{e n_e}$$

$$\frac{\partial \mathbf{B}}{\partial t} = -\nabla \times \mathbf{E} \sim -\frac{\nabla n_e \times \nabla T_e}{e n_e}$$

Azimuthal magnetic fields are generated by $\nabla n_e \times \nabla T_e$.

---

*K. Mima *et al.,* Phys. Rev. Lett., 41, 1715 (1978);
R. G. Evans, Plasma Phys. Control. Fusion., 28, 1021 (1986);
B. Srinivasan *et al.,* Phys. Rev. Lett., 108, 165002 (2012).
M. Manuel et al., Phys. Rev. Lett., 108, 255006 (2012).

Magnetic-field generation has been studied in side-on and face-on geometries using the acceleration of planar plastic targets

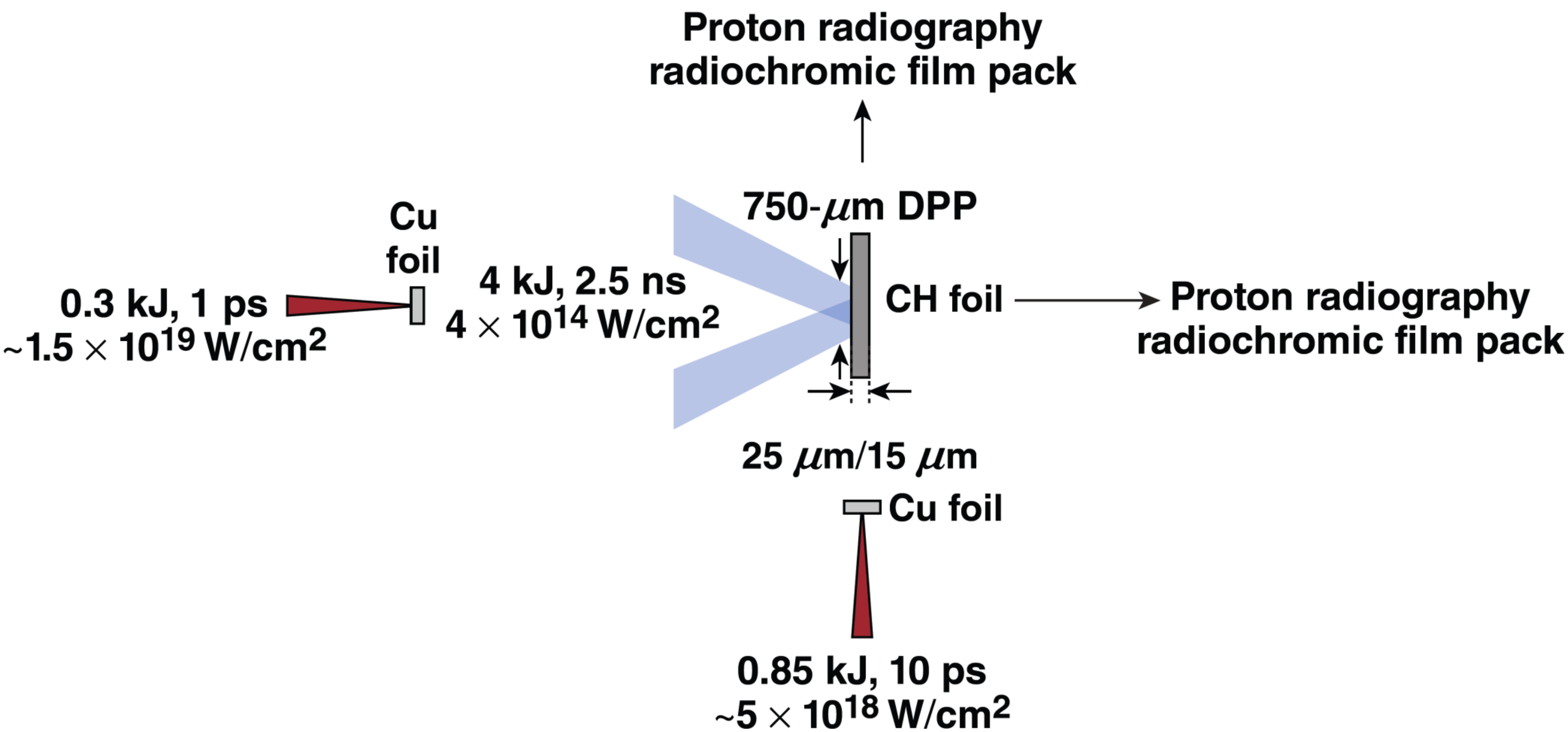

Side-on geometry

Proton radiography of 15-μm-thick foils reveals magnetic field generation and its evolution*

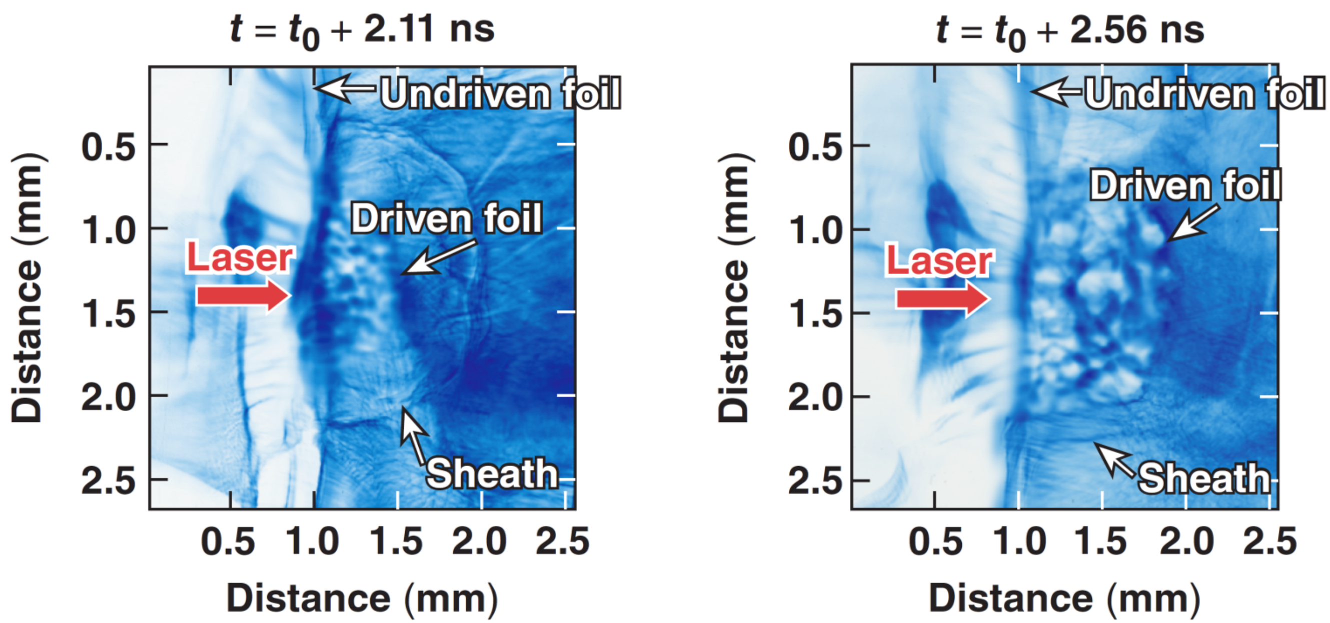

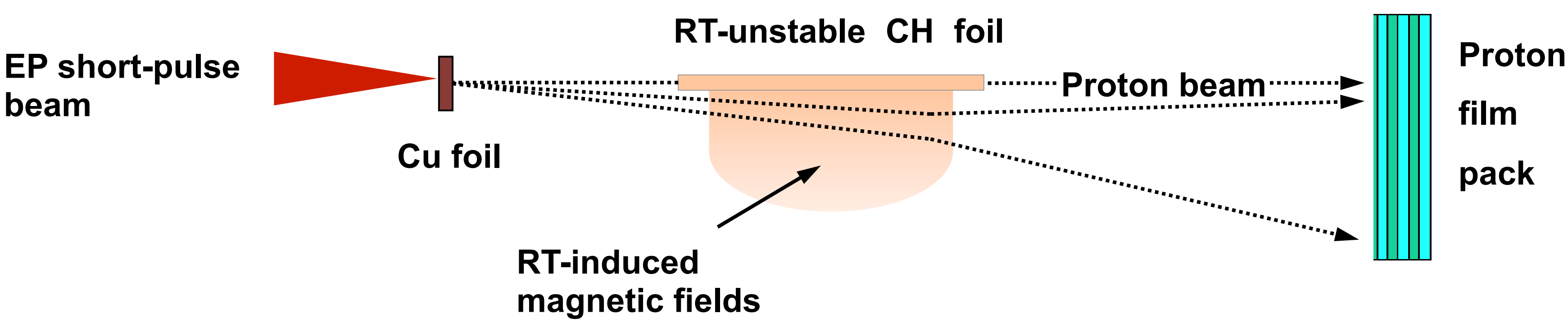

*L. Gao *et al.*, Phys. Rev. Lett. 109, 115001 (2012).

Face-on geometry

Face-on probing reveals magnetic field generation by the RT instability

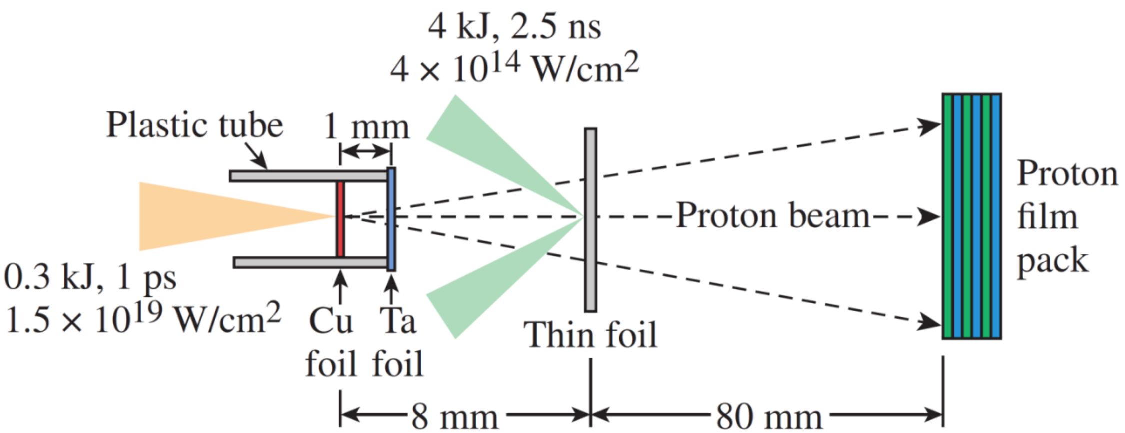

Proton radiograph

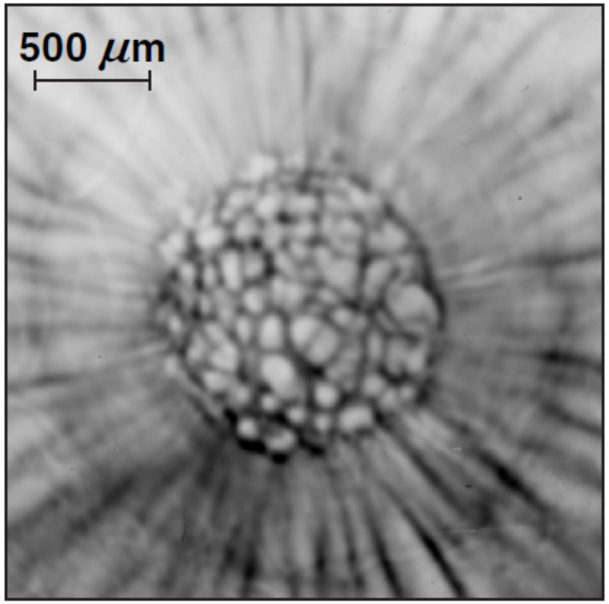

$t = t_0 + 2.6$ ns

Face-on geometry

The number of magnetic cells decreases and the magnetic cell diameter increases with time

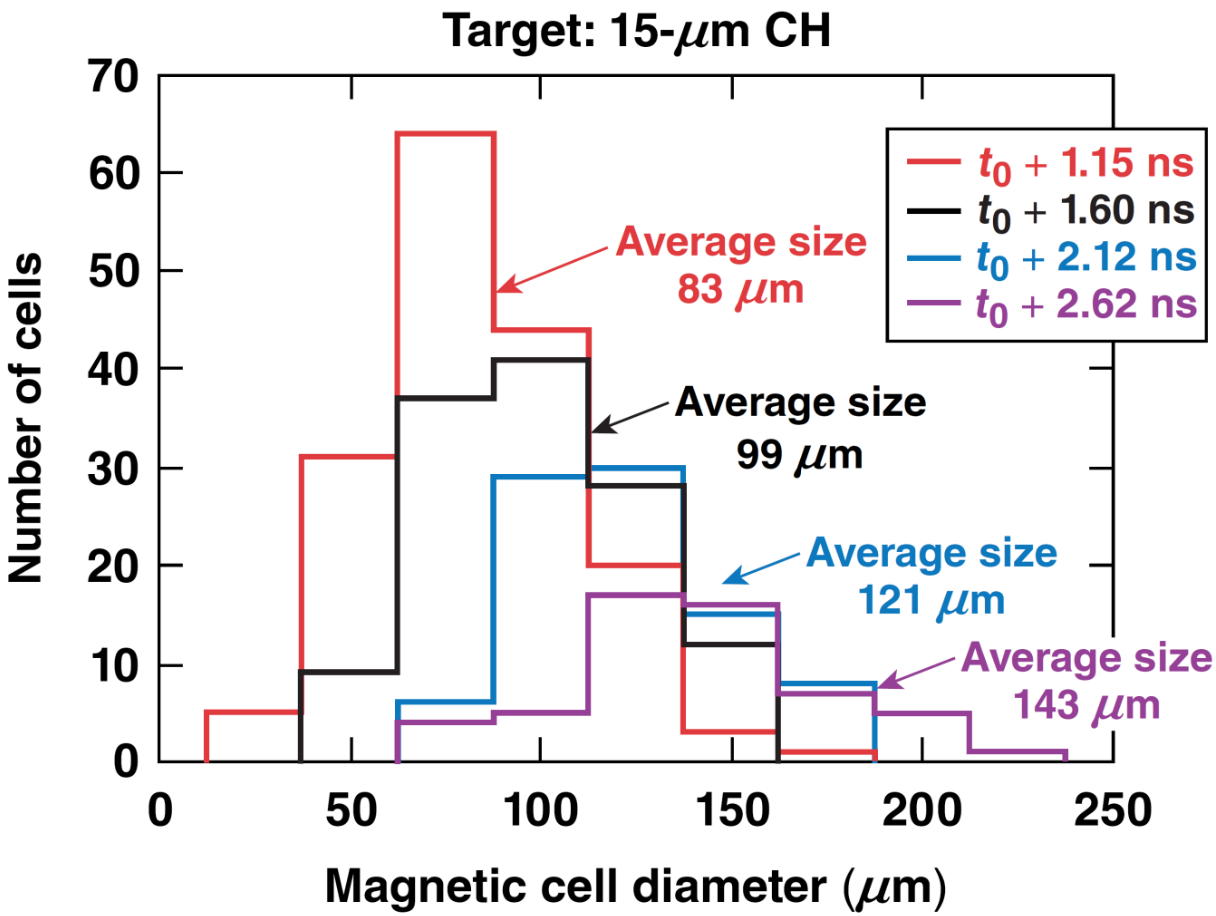

Face-on geometry

The normalized magnetic-field spatial distribution evolves self-similarly

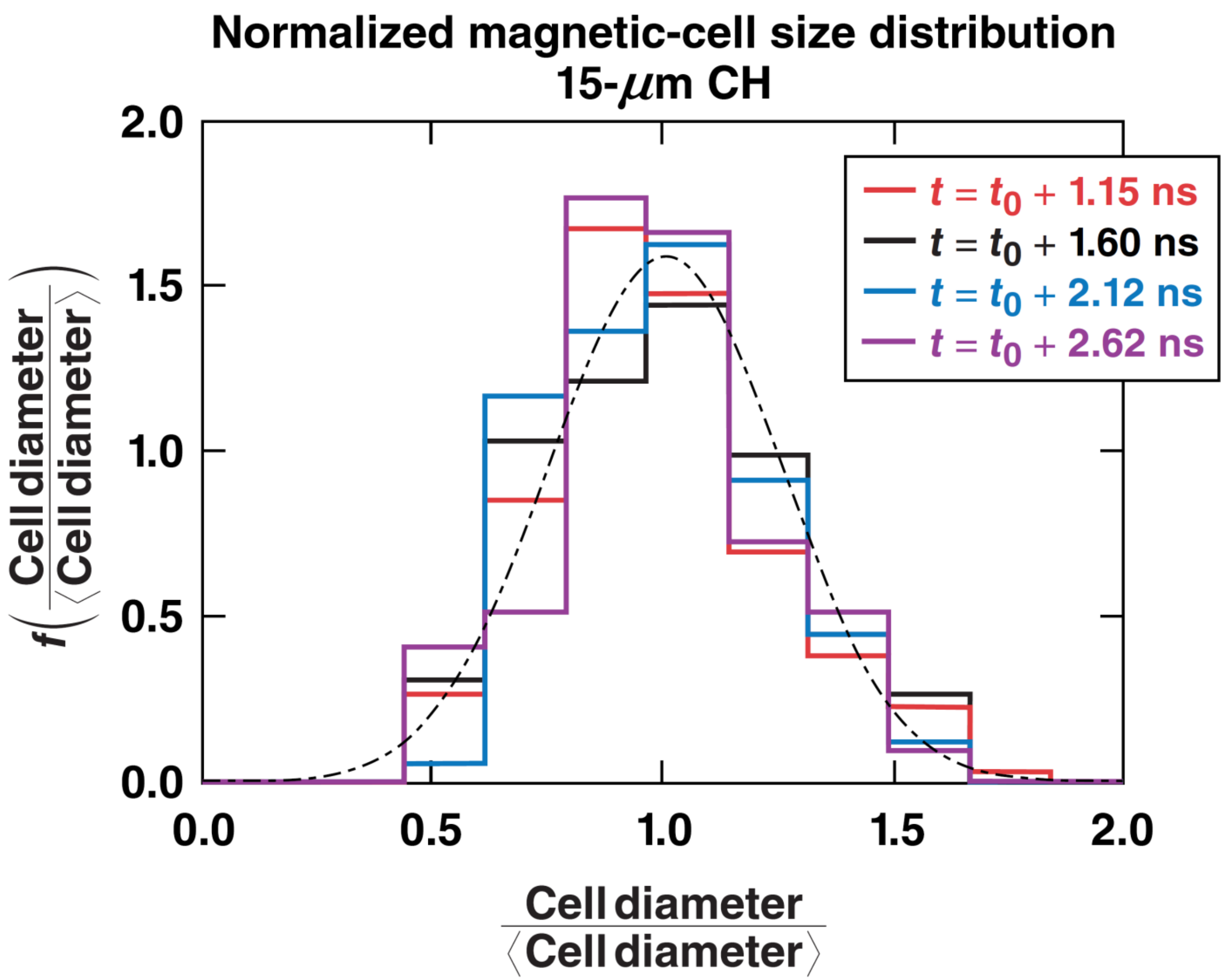

The evolution of the magnetic-field spatial distribution is consistent with an RT bubble competition and merger model*

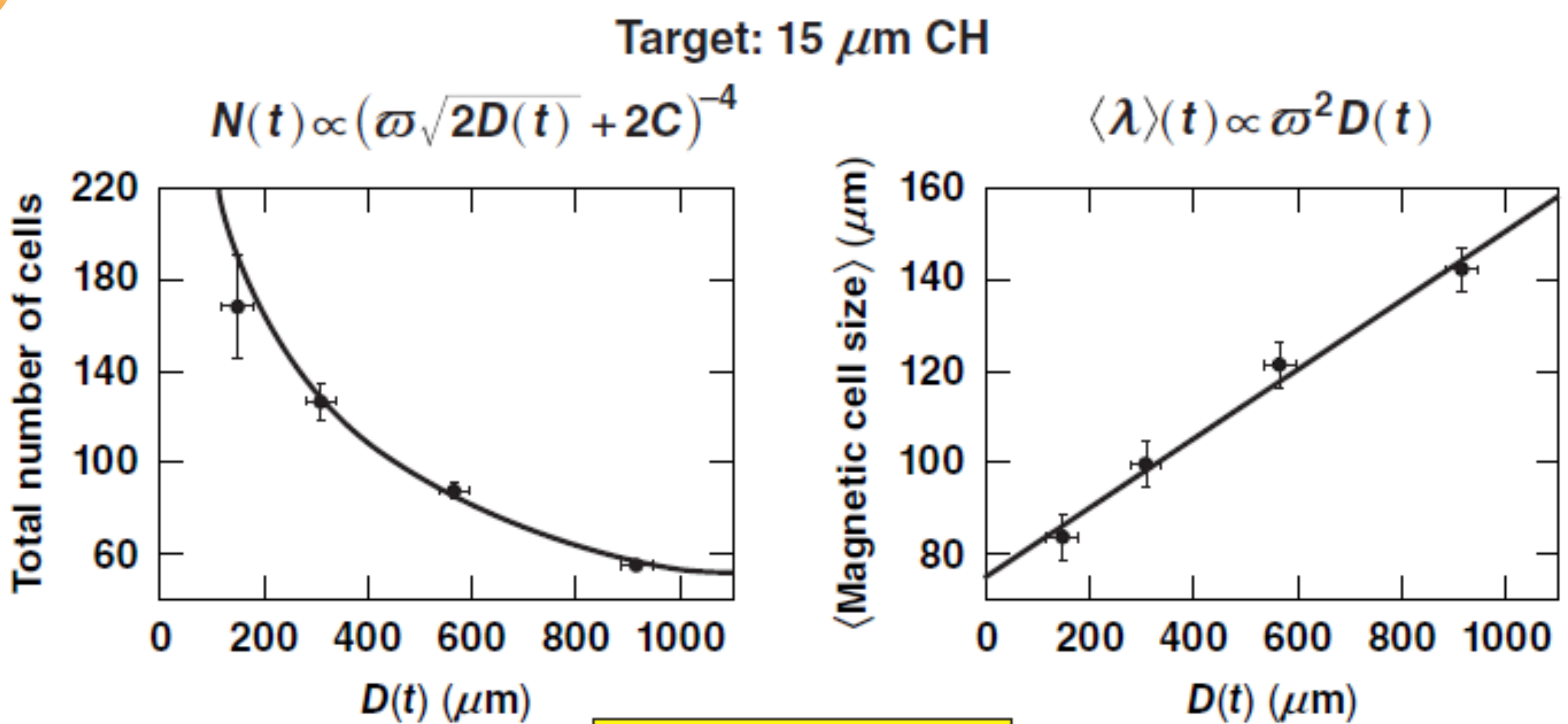

$\varpi_{CH} = 0.79 \pm 0.06$**

*O. Sadot *et al.*, Phys. Rev. Lett. 95, 265001 (2005); D. Oron *et al.*, Phys. Plasmas 8, 2883 (2001); U. Alon *et al.*, Phys. Rev. Lett. 72, 2867 (1994).

**L. Gao *et al.*, Phys. Rev. Lett. 110, 185003 (2013).

The origin and amplification of the magnetic field in the universe is a central astrophysical problem

- Sources of magnetic fields
- Amplification by the dynamo process
- Flow-dominated systems are common in astrophysics
- Particle acceleration, non-thermal emission

Dynamo

Two classes of experiments are proposed towards the first realization of a full MHD turbulence and dynamo in the HED systems using the NIF

Single RT plume

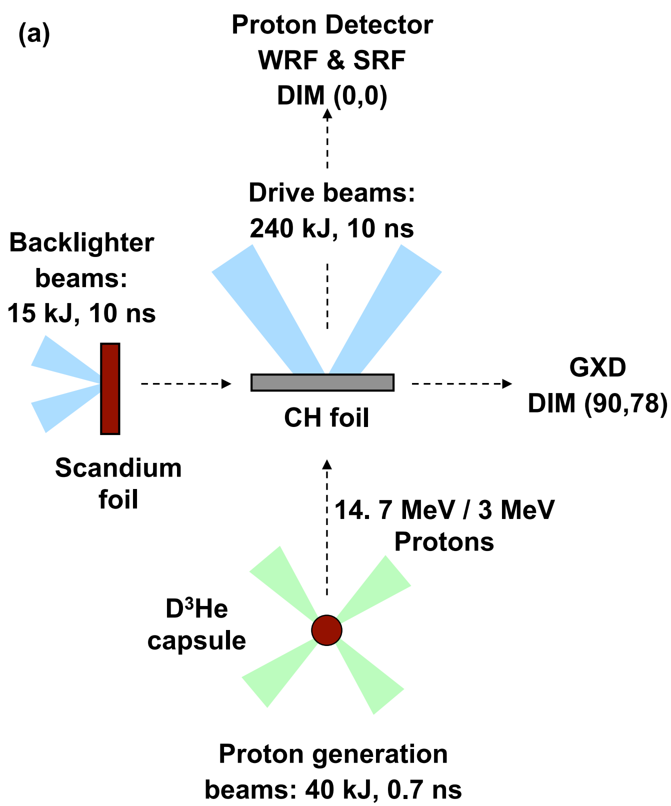

Colliding RT plumes

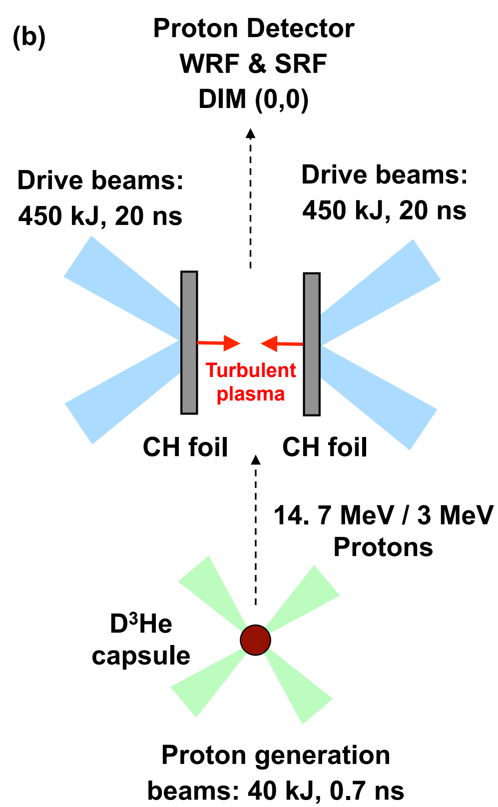

3D MHD simulation for the colliding case:

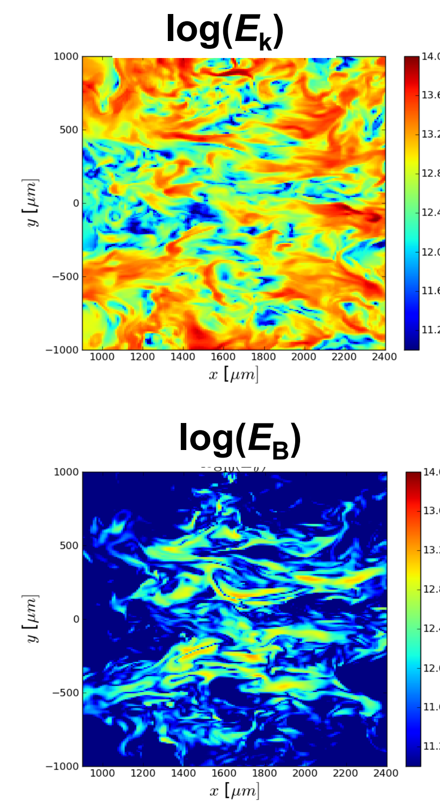

A D^3He mono-energetic proton radiography platform has been developed by MIT for HEDP experiments

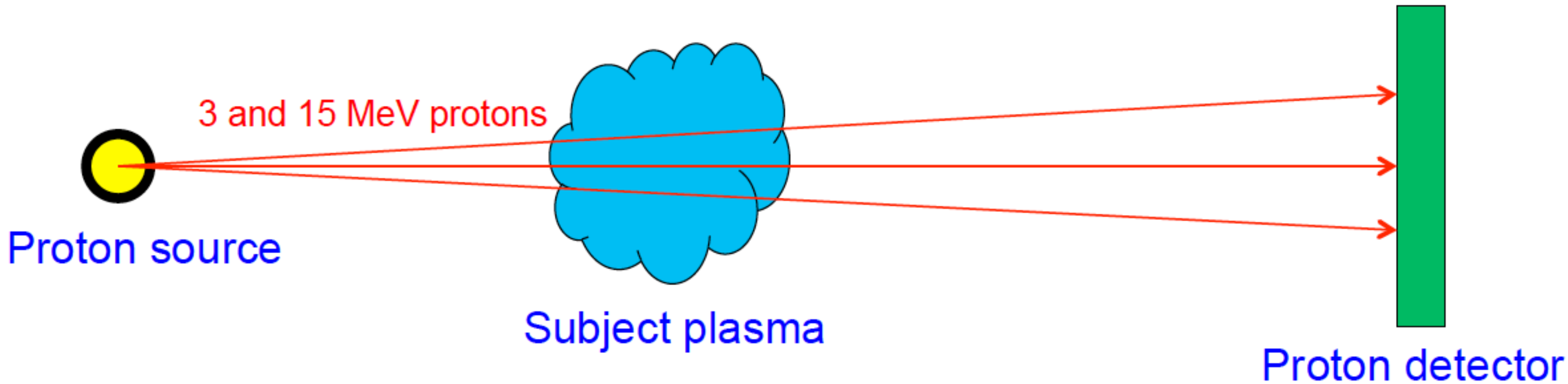

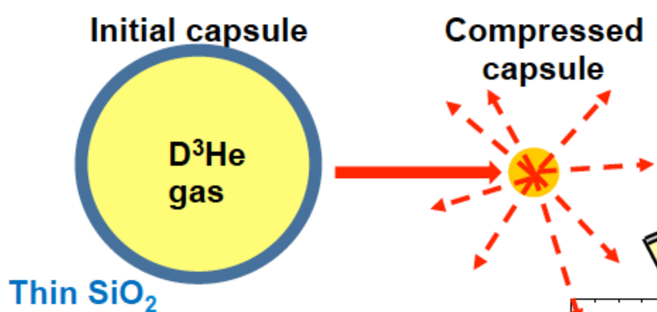

$D + {}^3He \rightarrow p(14.7\ MeV) + \alpha$

$D + D \rightarrow p(3.0\ MeV) + T$

$D + D \rightarrow n + {}^3He$

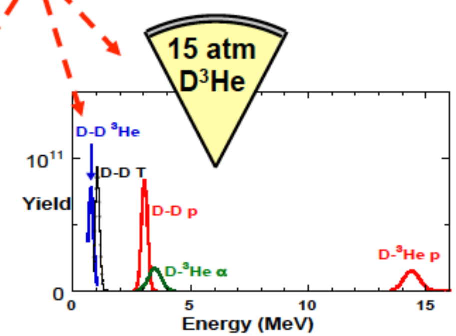

Spatial resolution: ~ 40 μm (FWHM)
Energy resolution: ~ 3%
Temporal resolution: ~ 80 ps

C. K. Li *et al.*, Phy .Rev. Lett. (2006)
C. K. Li *et al.*, Rev.Sci.Instrum (2006)
F. Seguin *et al.*, Rev.Sci.Instrum (2003)

A strong, fast propagating, magnetized jet has been created at the OMEGA Laser Facility

Magnetized Jet and the Collisionless Shock

OMEGA Experiment

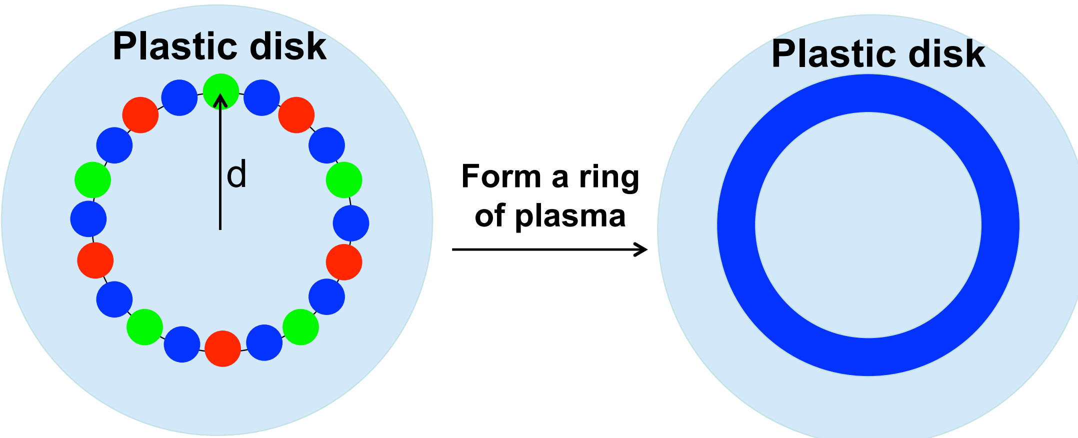

- P1 axis, Ring 1, 5 beams
- P1 axis, Ring 2, 5 beams
- P1 axis, Ring 3, 10 beams

d = 0, 400 um, and 800 um

Magnetized Jet measured by D^3He protons

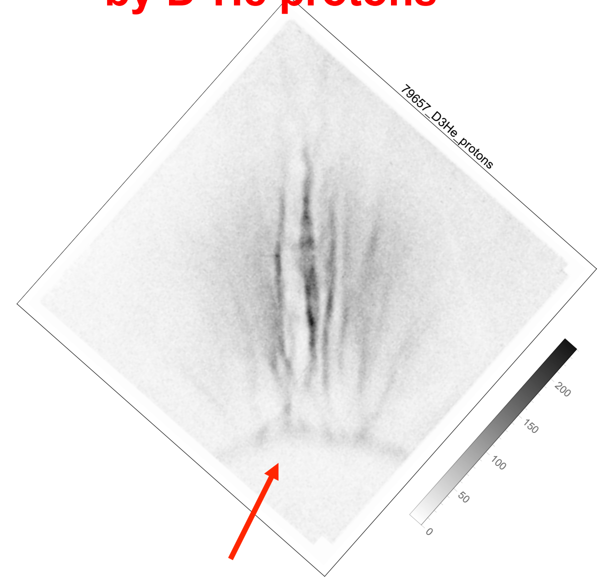

Plastic disk

- Collisionless shocks are believed to sites for cosmic ray acceleration
- A magnetized, supersonic jet has been successfully demonstrated in the FY16 campaign, in collaboration with Rice, LLE and MIT
- The next goal is to collide the jets for collionless shock

Precision mapping of the laser-driven magnetic fields

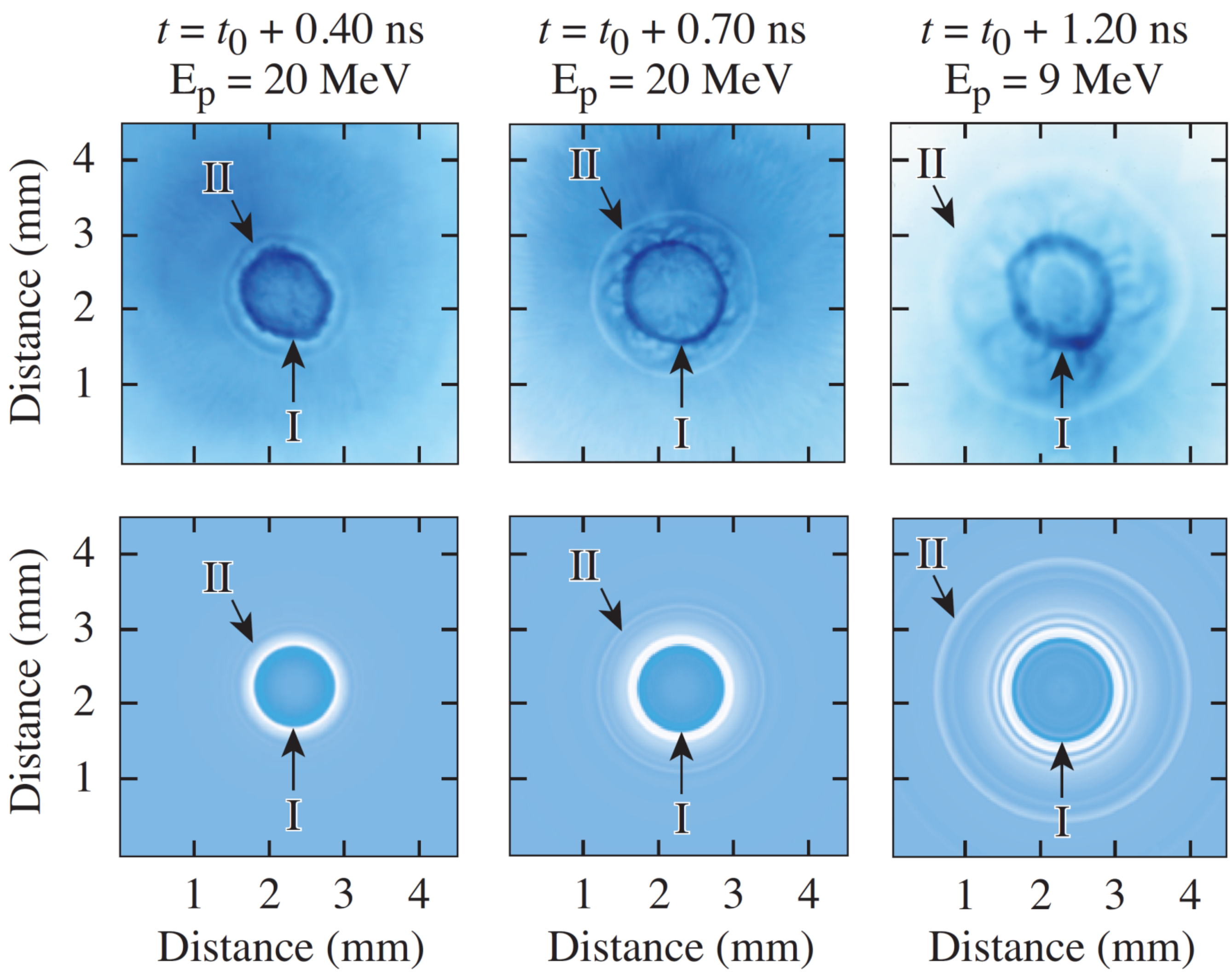

*L. Gao *et al.*, Phys. Rev. Lett. 114, 215003 (2015).

Ultrafast proton radiography directly measured 100s of Tesla magnetic fields generated by a laser-driven capacitor coil target

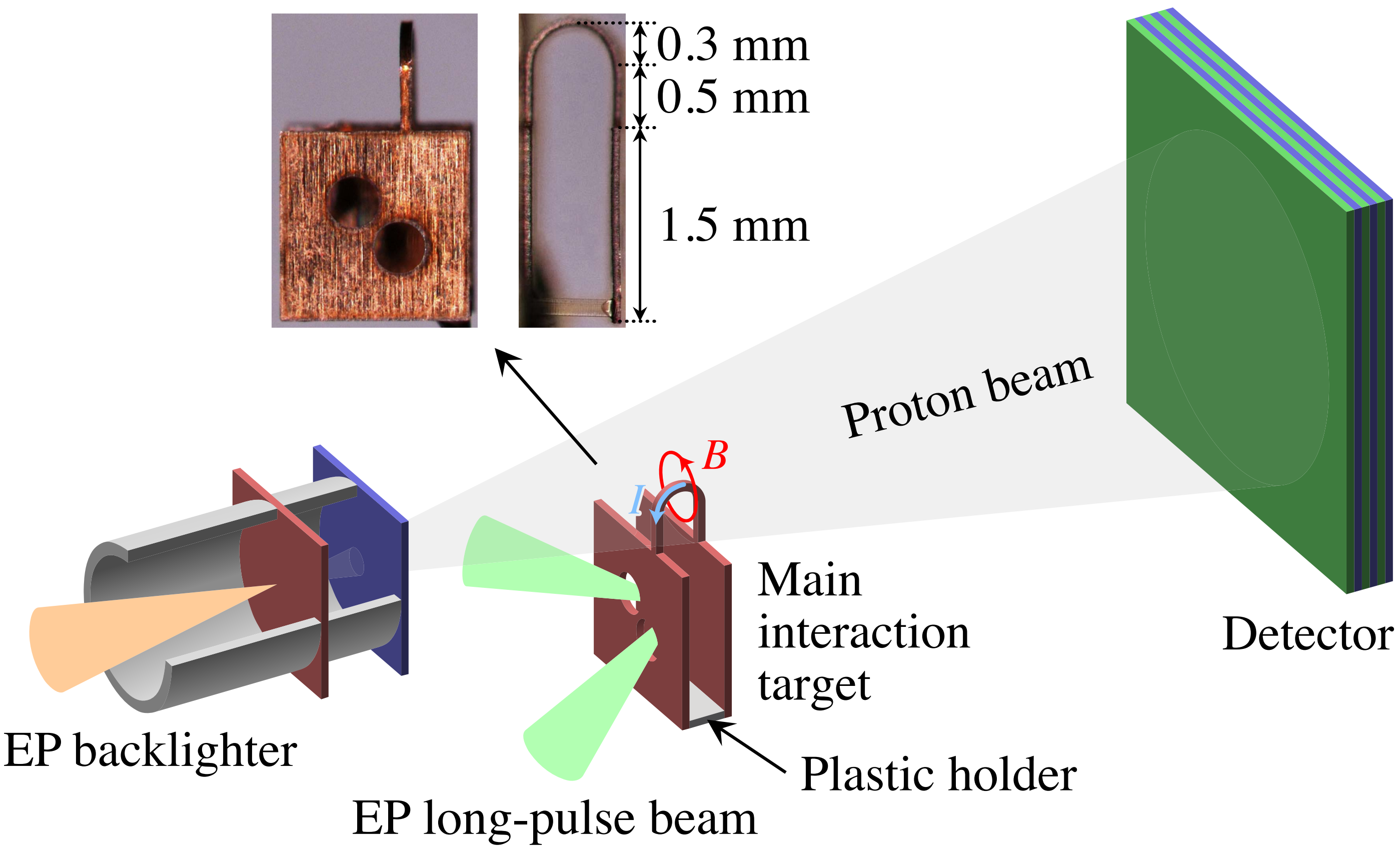

*L. Gao *et al.*, Phys. Plasma 23, 043106 (2016)

Outline

- Basic diagnostic building blocks
  - Electromagnetic field
    - Proton radiography
  - Particles
    - RCF stack / Proton activation pack / Electron spectrometer / Thomson parabola
  - X rays
    - Pinhole camera (time integrated) / 1-D streak camera / 2-D framing camera
  - Plasma conditions
    - High-resolution x-ray spectroscopy / Thomson scattering / Neutrons / x-ray radiography

Radiochromic film allows simple detection of high-energy photons and particles

- Radiochromic film is self-developing and insensitive to visible light
- Multiple layers of film and filters allow energy discrimination

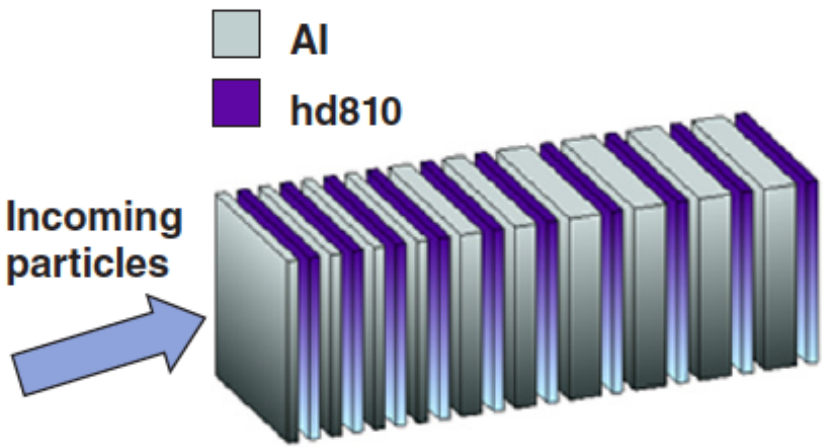

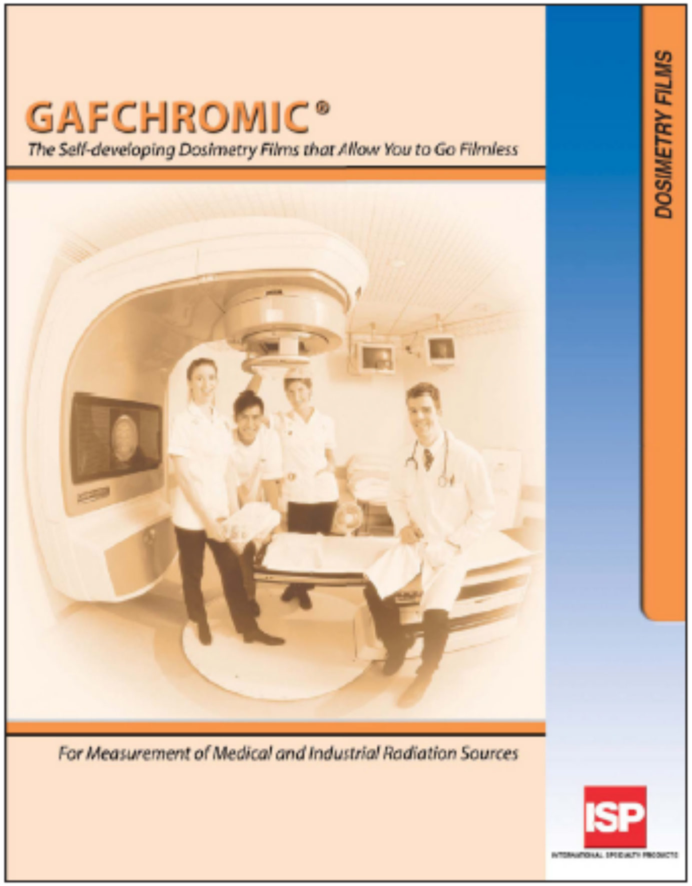

Experiments were performed on OMEGA EP to characterize energetic protons

Focal spot (R_{80})	20 ~ 25 μm
Laser energy	40 J ~ 1500 J
Intensity (average within R_{80})	0.25 ~ 8 × 10^{18} W/cm^2
Intensity contrast	~10^8
Targets	500 μm^2 × 20 μm Cu/Cu+Al/Cu+CH 500 μm^2 × 50 μm Cu

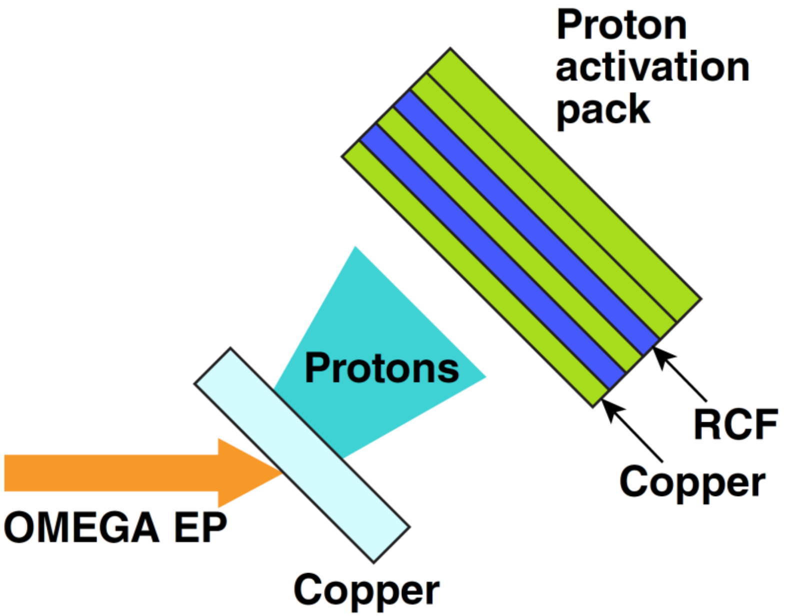

Nuclear activation of copper stacks determined the energy spectrum of the forward-accelerated protons

- Radiochromic film shows proton beam profile
- ^{63}Cu (p, n) ^{63}Zn
  ^{65}Cu (p, 3n) ^{63}Zn
- Coincidence counter absolutely calibrated using known source Na_{22}
- Response functions using stopping power* and cross-section data**
- An iterative method to recover the energy spectrum

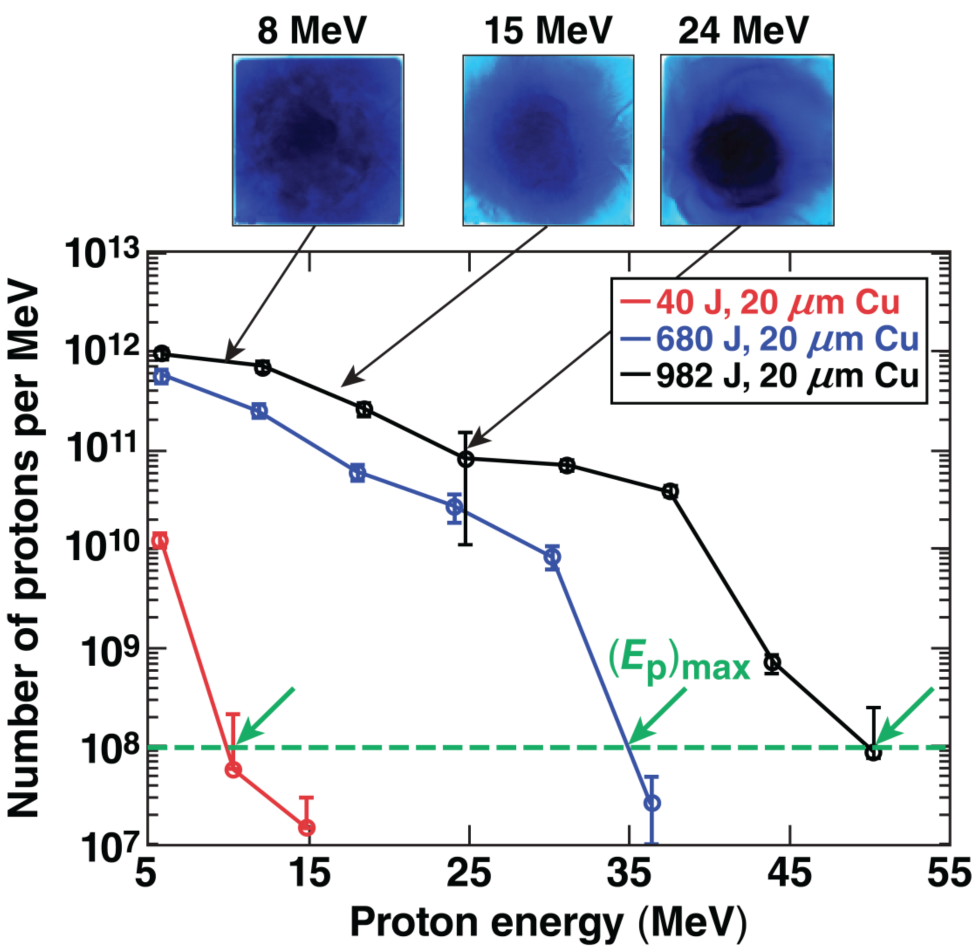

* http://physics.nist.gov/Star.
** http://www.nndc.bnl.gov/exfor/.

Nuclear activation of copper stacks determined the energy spectrum of the forward-accelerated protons

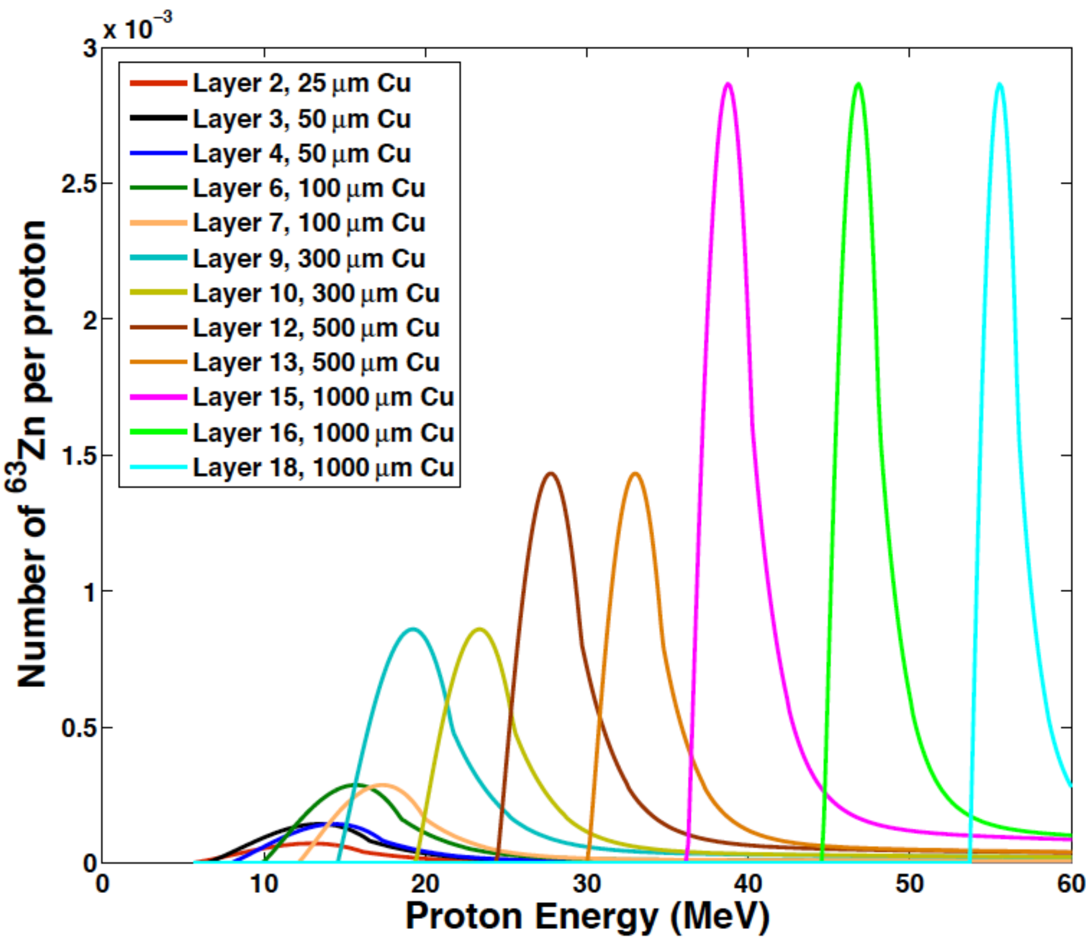

The energy spectrum of high-energy charged particles can be measured with a magnetic spectrometer

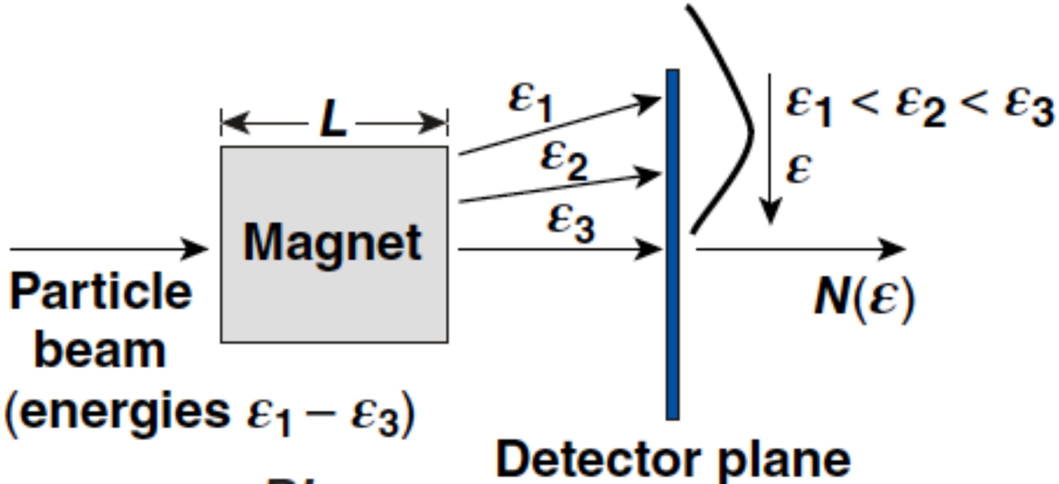

$$\tan\theta = \frac{qBL}{c\sqrt{2m\varepsilon}}$$

- Some issues
  - must know the detector response as a function of ε
  - $\frac{\Delta\varepsilon}{\varepsilon}$ is smaller at higher energy
  - the design can be optimized
    - magnet geometry
    - detector-plane orientation

- A major limitation is that the spectrometer cannot resolve among particles with the same sign of charge but different q, m, ε degenerate

- A magnetic spectrometer works well for
  - electrons, positrons
  - ions when only a single species is present—typically protons

The energy spectrum of high-energy charged particles can be measured with a magnetic spectrometer

OU-ESM

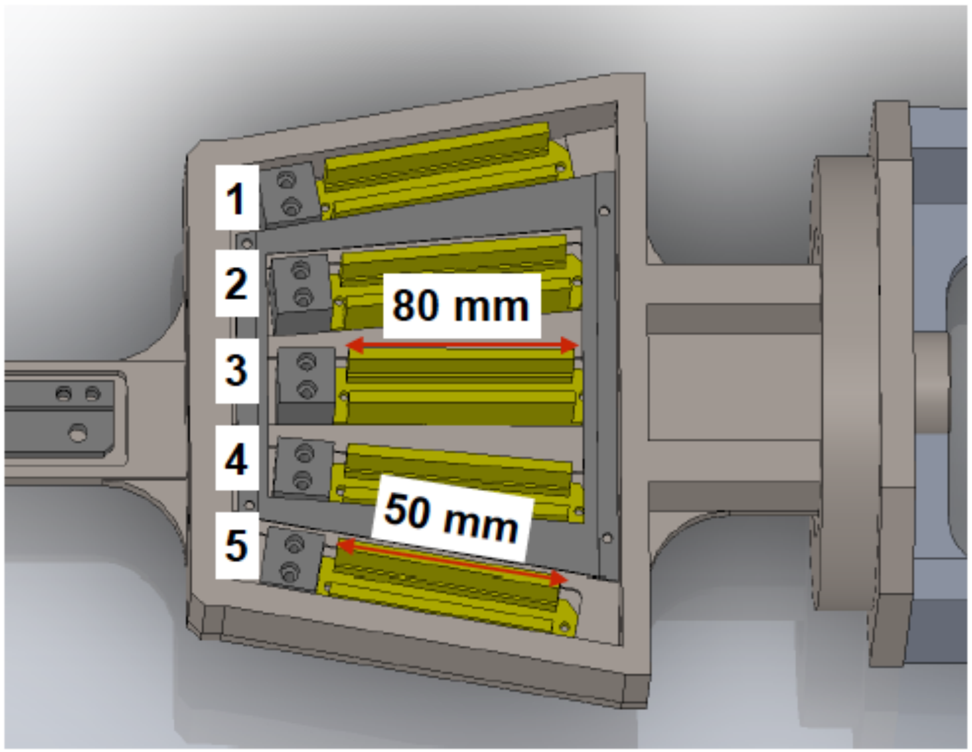

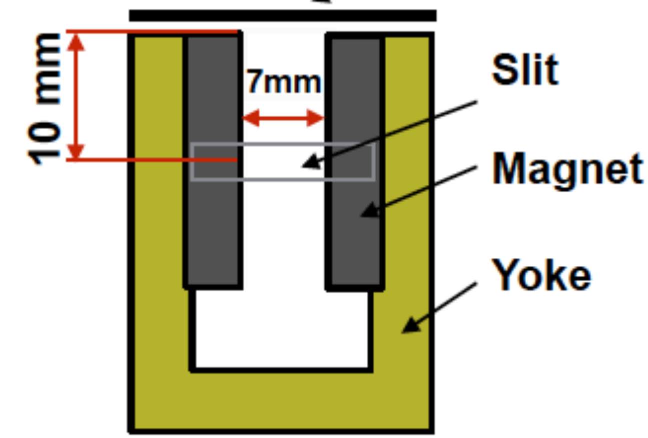

Ch1 -10°	50 mm length
Ch2 -5°	80 mm length
Ch3 -0°	80 mm length
Ch4 +5°	80 mm length
Ch5 +10°	50 mm length

A Thomson parabola uses parallel electric and magnetic fields to deflect particles onto parabolic curves that resolve q/m

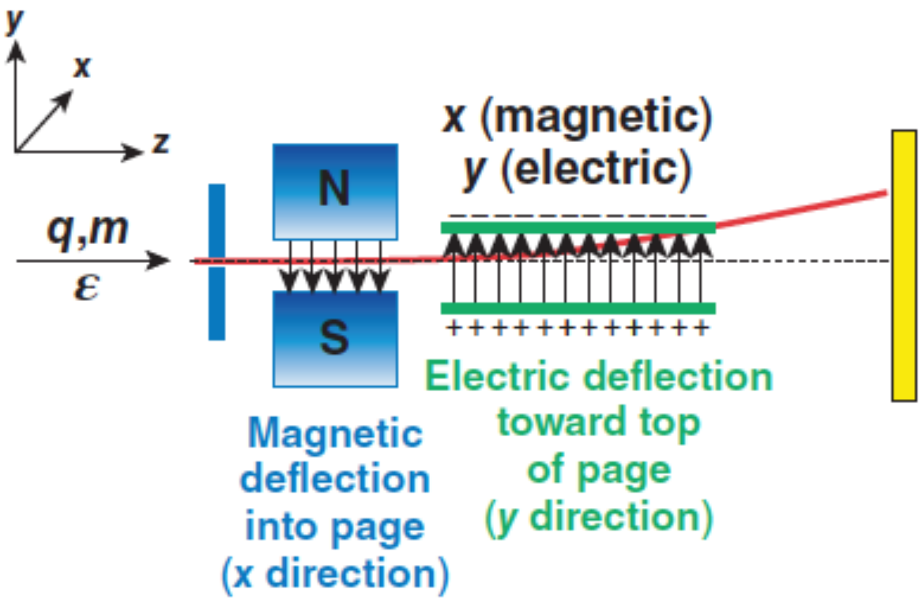

- Deflection caused by magnetic field ~q/p
- Deflection caused by electric field ~q/KE
- Ion traces form parabolic curves on detector plane

$$y = \frac{mc^2 E}{qLB^2} x^2$$

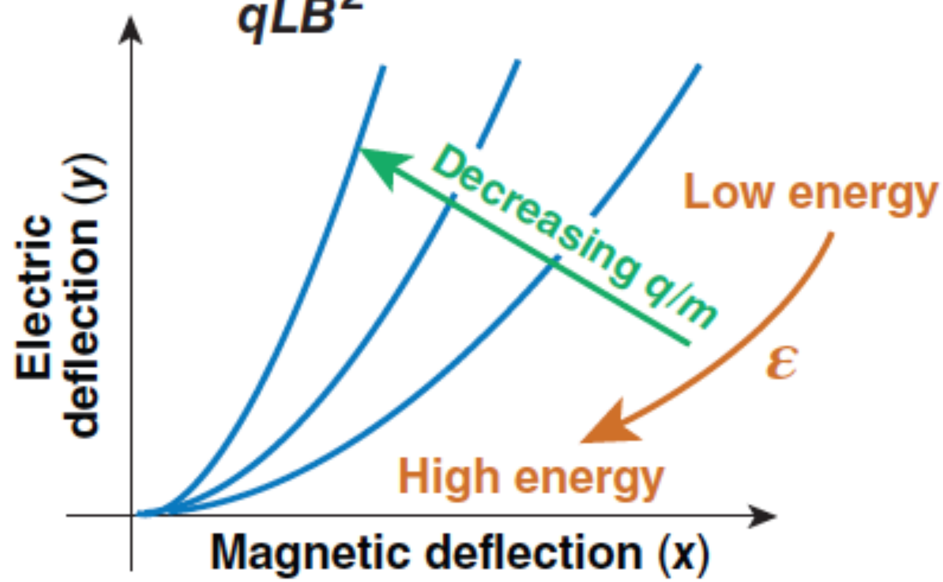

$$\tan \Delta\theta_x = \Delta\theta_x = \frac{qBL}{c\sqrt{2m\varepsilon}}$$

y deflection

$$F_\perp = qE$$

$$\Delta m V_y = qE\tau = \frac{qEL}{V}$$

$$\tan\theta_y \sim \theta_y = \frac{\Delta m V_y}{mV} = \frac{qEL}{2\varepsilon}$$

Outline

- Basic diagnostic building blocks
  - Electromagnetic field
    - Proton radiography
  - Particles
    - RCF stack / Proton activation pack / Electron spectrometer / Thomson parabola
  - X rays
    - Pinhole camera (time integrated) / 1-D streak camera / 2-D framing camera
  - Plasma conditions
    - High-resolution x-ray spectroscopy / Thomson scattering / Neutrons / x-ray radiography

The simplest imaging device is a pinhole camera

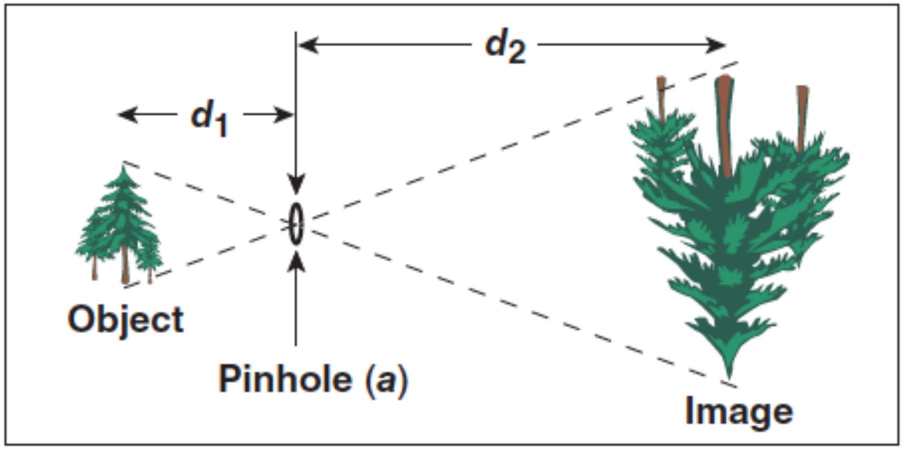

Kodak Brownie camera

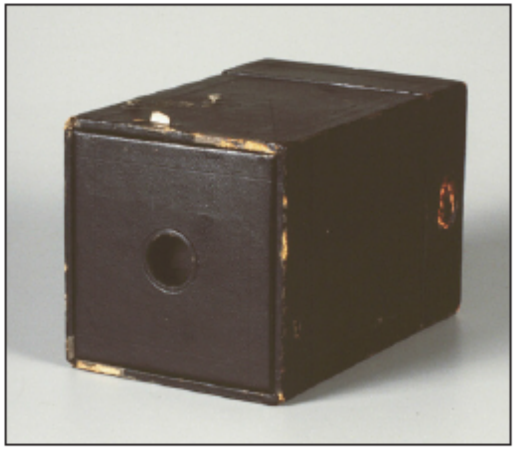

- Magnification $= \dfrac{d_2}{d_1}$
- Infinite depth of field (variable magnification)
- Pinhole diameter determines
  - resolution $\sim a$
  - light collection: $\Delta\Omega = \dfrac{\pi}{4}\dfrac{a^2}{d_1^2}$

Imaging optics (e.g., lenses) can be used for higher resolutions with larger solid angles.

E13982a

2-D time-integrated images can be recorded on film or electric detectors

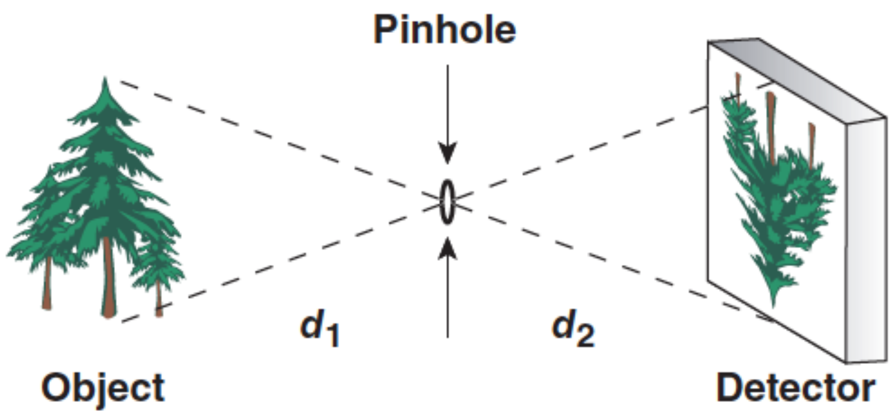

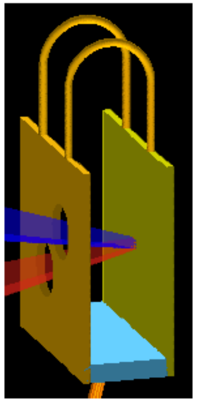

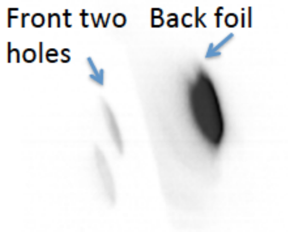

- A 2-D detector is required for a pinhole camera
  - film—requires processing
  - electronic
    - semiconductor arrays—signal proportional to incident flux per pixel (CCD or CID)
    - array of ionization detectors
    - single-photon counters—limited dynamic range

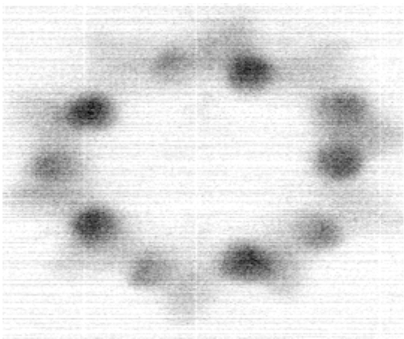

A framing camera provides a series of time-gated 2-D images, similar to a movie camera

- The building block of a framing camera is a gated microchannel-plate detector (MCP).
- An MCP is a plate covered with small holes.

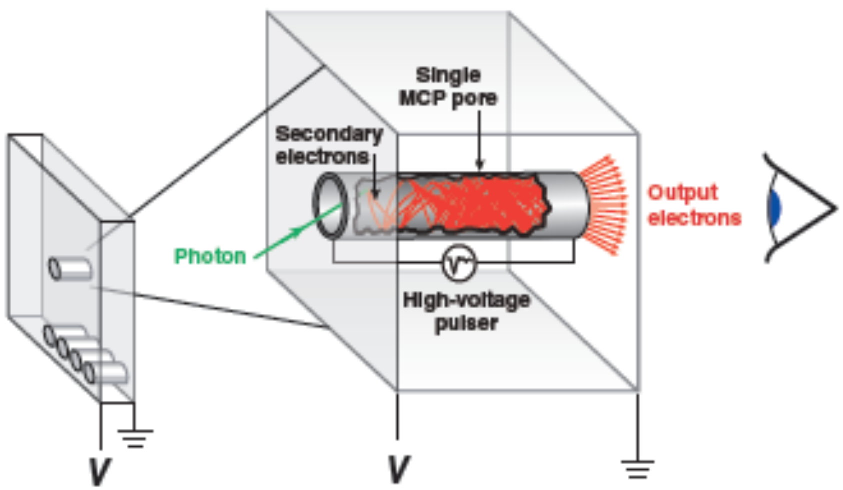

Multiple electrons are produced each time an electron or photon hits the wall.

Two-dimensional time-resolved images are recorded using x-ray framing camera

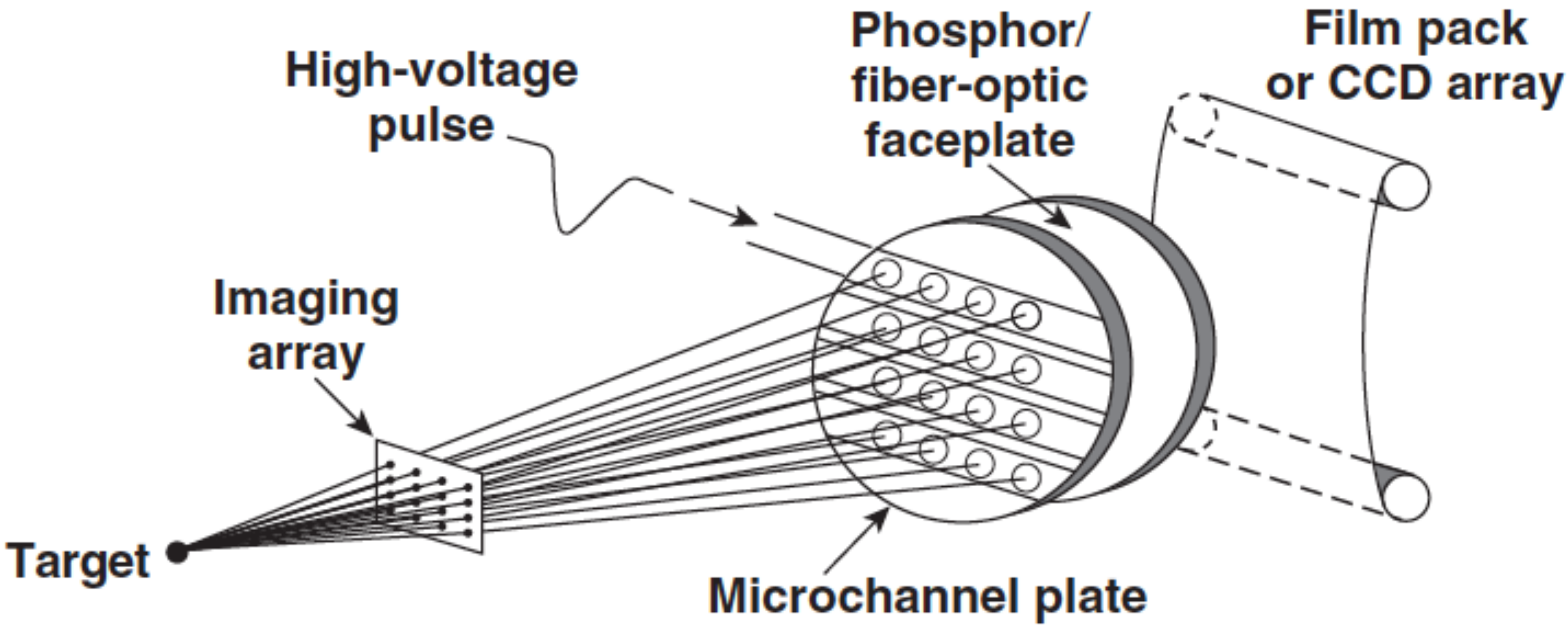

- Temporal resolution = 35 to 40 ps
- Imaging array: Pinholes: 10- to 12-μm resolution, 1 to 4 keV
- Space-resolved x-ray spectra can be obtained by using Bragg crystals and imaging slits

Two-dimensional time-resolved images are recorded using x-ray framing camera

X-ray framing camera: self-emission of the magnetized jet

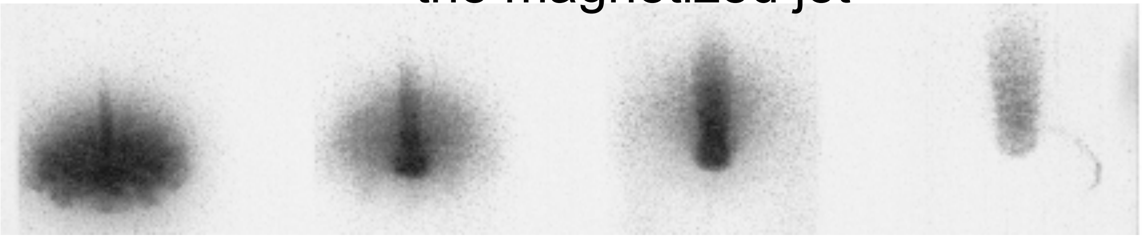

Proton radiography: magnetic fields around the magnetized jet

NIF’s gated x-ray framing camera DIXI has 10-ps temporal resolution and observes features not seen with NIF’s last century gated x-ray cameras

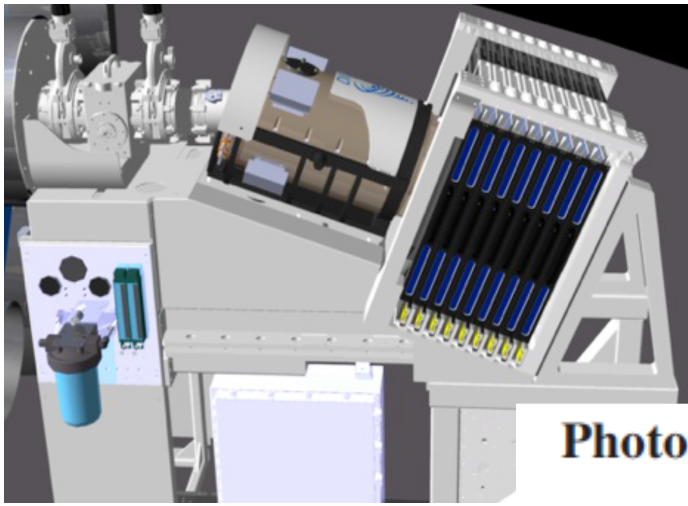

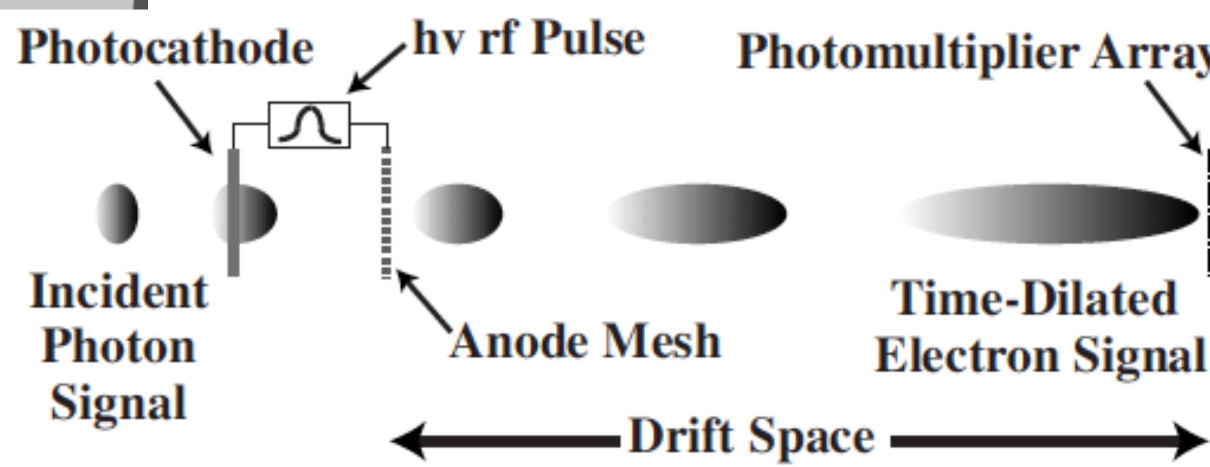

*T. J. Hilsabeck et al., RSI 81, 10E317 (2010)

DIXI takes clearer pictures of the hot spot evolution around peak x-ray emission

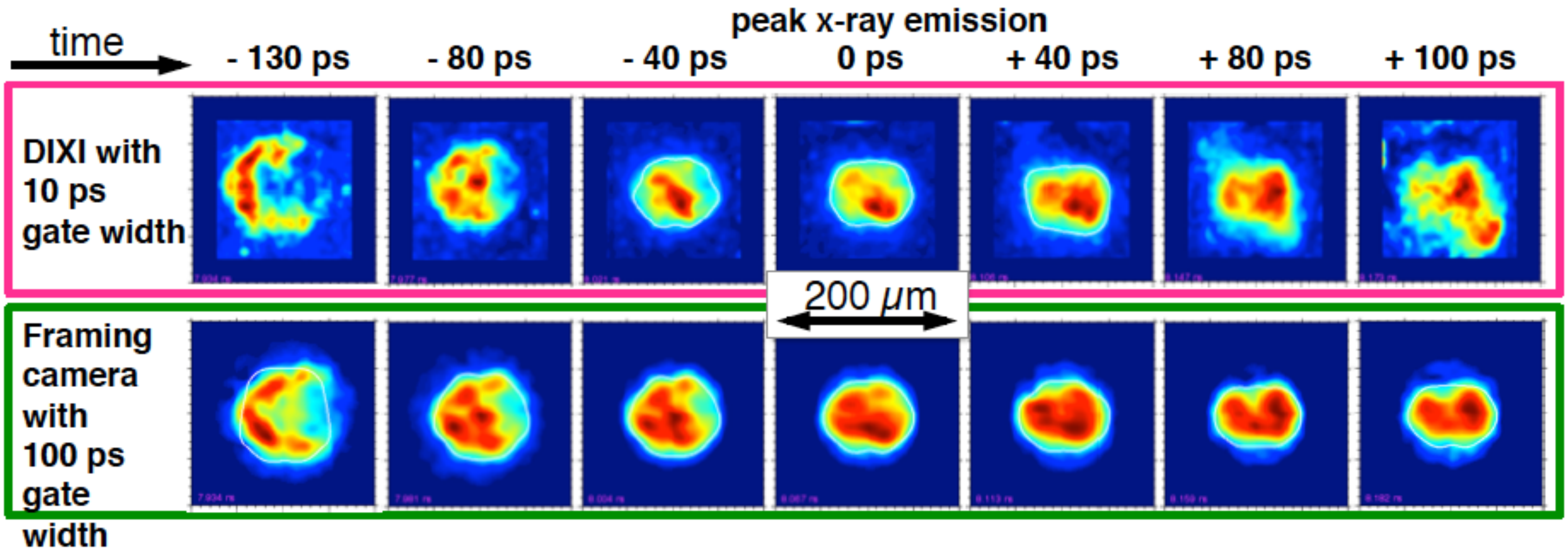

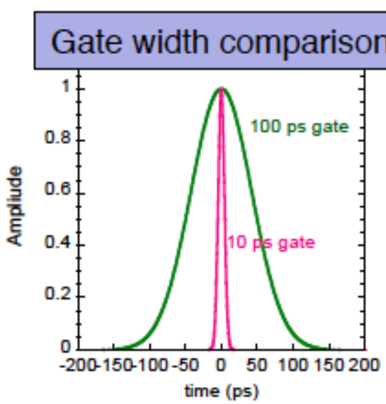

DIXI's 10X higher temporal resolution (reduced temporal blur) reveals details in the evolution of implosions at NIF never before possible, using the slower cameras.

N141116

A streak camera provides temporal resolution of 1-D data

Basic principle

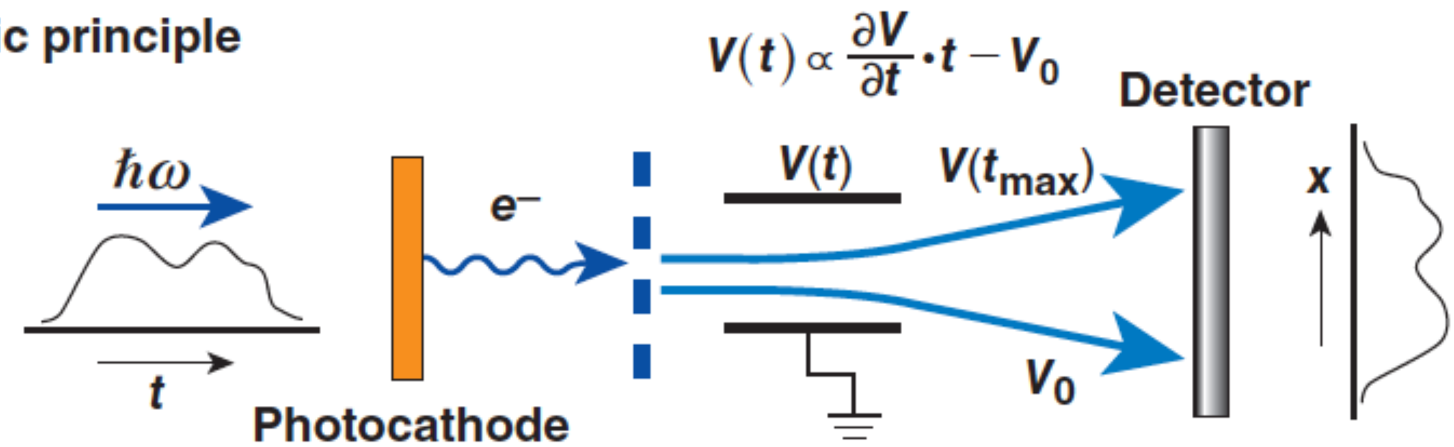

A streak camera can provide 2-D information

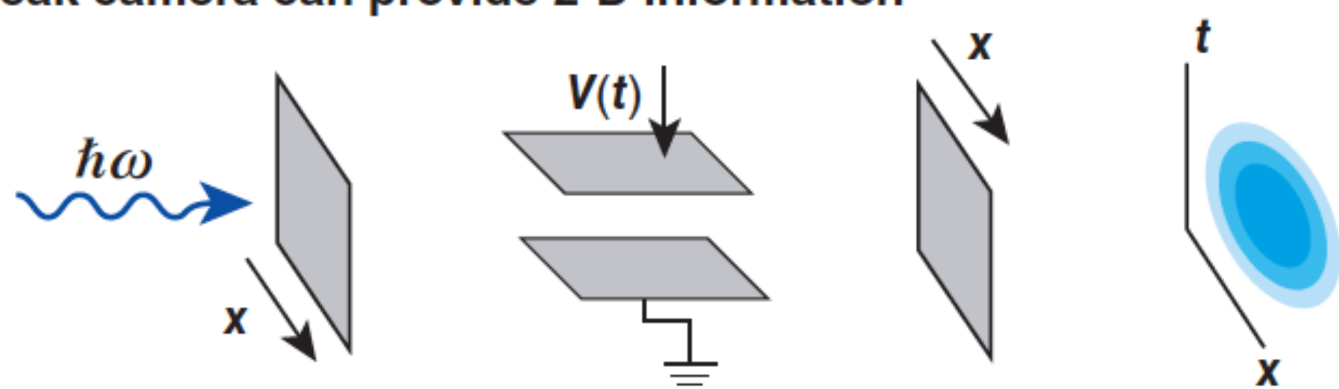

Outline

- Basic diagnostic building blocks
  - Electromagnetic field
    - Proton radiography
  - Particles
    - RCF stack / Proton activation pack / Electron spectrometer / Thomson parabola
  - X rays
    - Pinhole camera (time integrated) / 1-D streak camera / 2-D framing camera
  - Plasma conditions
    - High-resolution x-ray spectroscopy / Thomson scattering / Neutrons / x-ray radiography

High-resolution x-ray spectroscopy is well-established on Tokamaks for measuring plasma conditions

Horizontal: $\frac{1}{p_m} + \frac{1}{q_m} = \frac{2}{R\sin\theta}$

Vertical: $\frac{1}{p_s} + \frac{1}{q_s} = \frac{2\sin\theta}{R}$

astigmatism (different H/V focal lengths)

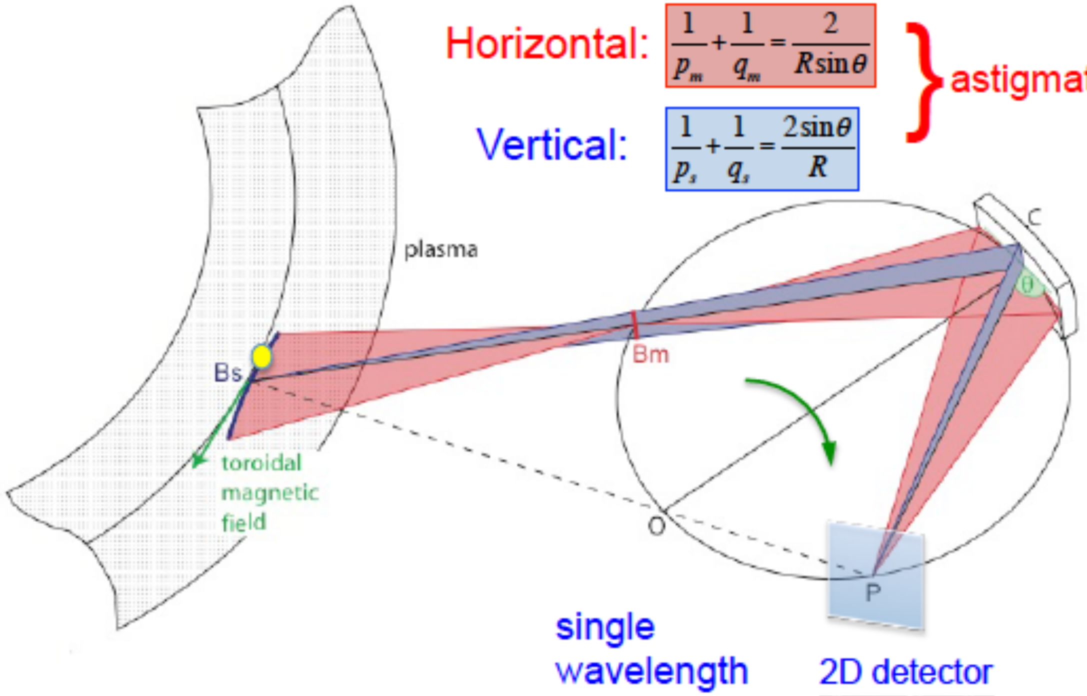

spherically
bent crystal

Bragg relation
$n\lambda = 2d\sin\theta$

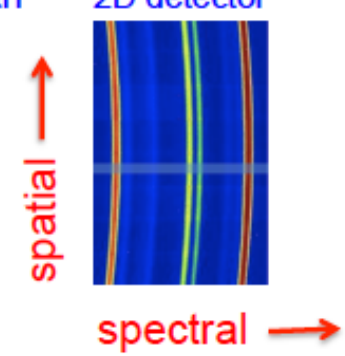

Can obtain spatial resolution for small sources if the source is located on the sagittal focal line at Bs.

Enabling Principles

- Astigmatism of a spherical reflector
- Bragg relation
- Rotational symmetry of a spherical reflector about the normal axis, CO

High-resolution x-ray spectroscopy is well-established on Tokamaks for measuring plasma conditions

PPPL digest
PRINCETON PLASMA PHYSICS LABORATORY
A United States Department of Energy Facility
AUGUST 2007

X-ray Crystal Spectrometer Makes Debut at C-Mod

New Technique a Major Advance for ITER

A PPPL/Alcator C-Mod collaboration has resulted in the demonstration of a greatly improved X-ray crystal spectrometer for application to ITER and fusion reactors. Experiments conducted by a PPPL/MIT team in April mark the beginning of a new era in the ability of such devices to determine radial profiles of the ion temperature and the rotational velocity of high temperature plasmas without the need for diagnostic beams. Their success will benefit substantially ITER and other advanced fusion energy systems.

From the left are: Alex Ince-Cushman, MIT; Ken Hill, PPPL; Manfred Bitter, PPPL; John Rice, MIT; and Christian Broennimann of the Paul Scherrer Institute in Switzerland.

impurity by the pattern of frequencies, or spectrum, of the light emitted and they can determine the

PPPL designed high-resolution x-ray spectrometer has been identified as one of the 8 National Transformative Diagnostics

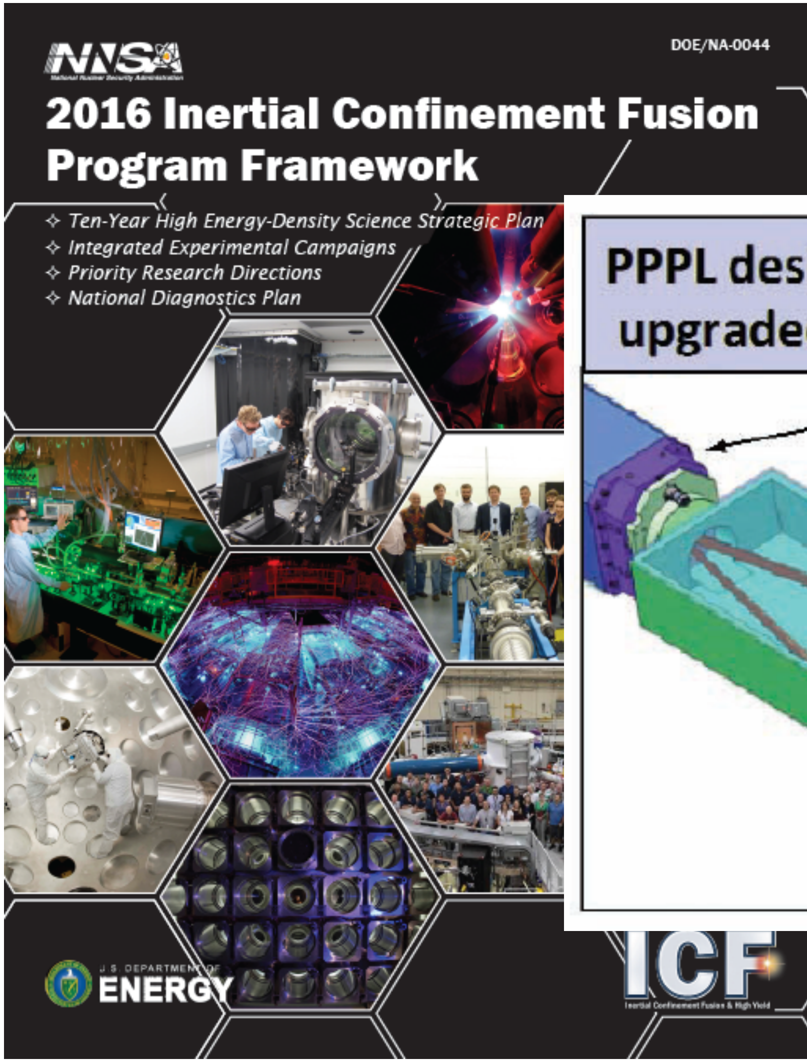

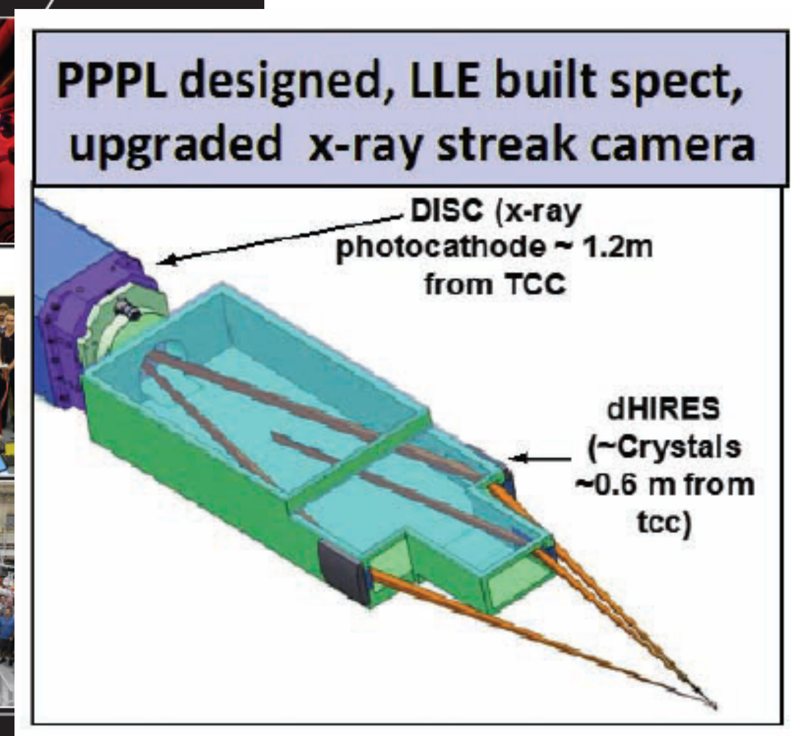

DHIRES contains three spectrometer channels and one imaging channel

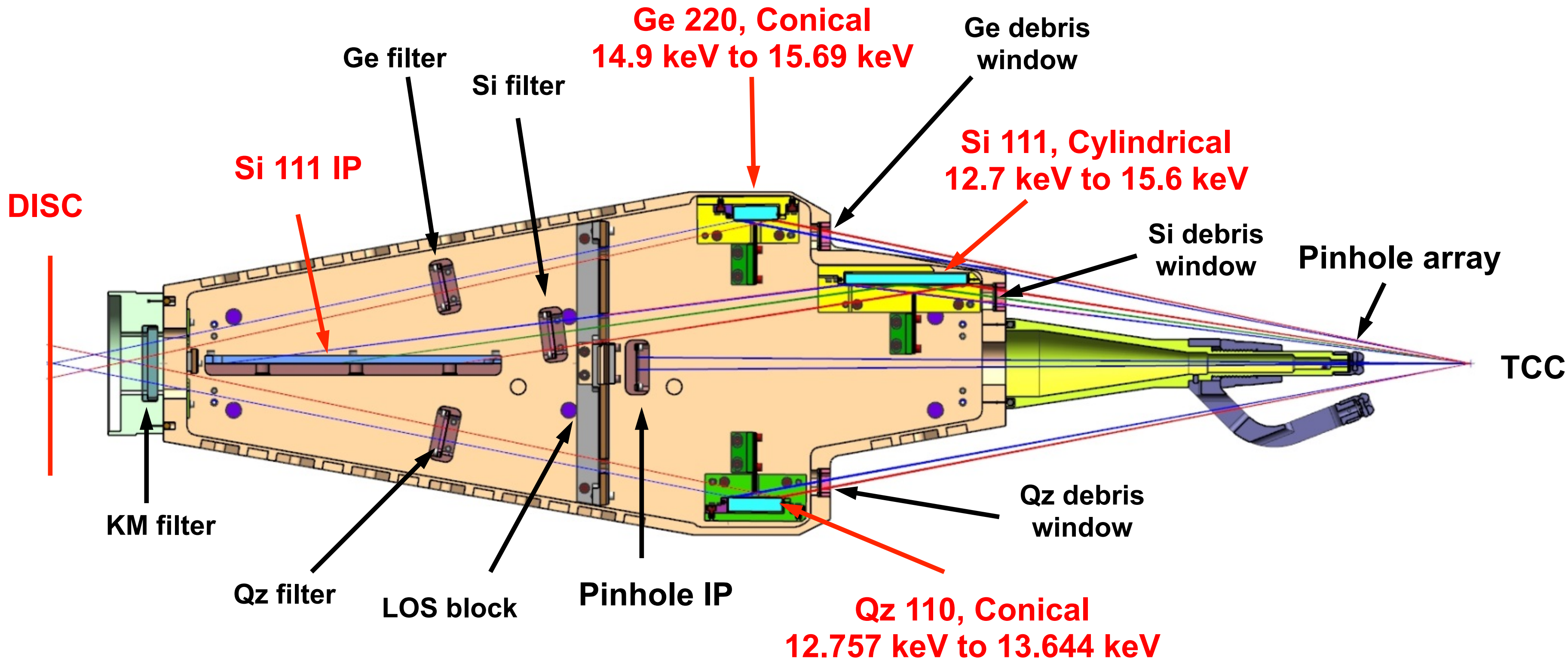

T. Hall geometry: J.Phys. E. 17, 110 (1984)

DHIRES contains three spectrometer channels and one imaging channel

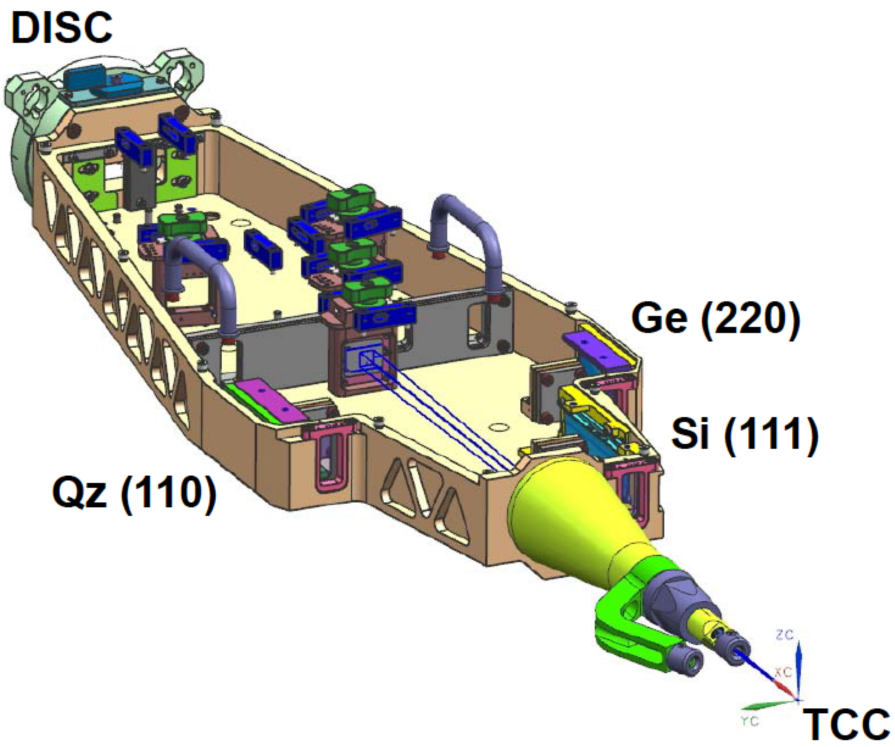

DHIRES is fully calibrated at the PPPL x-ray lab*

- Source Alignment
- Crystal Evaluation
- Energy Calibration and Crystal Dispersion
- Spectrum Manipulation
- Source Displacement and Insertion Error
- Absolute Throughput Measurement and NIF Signal Level Prediction
- Optical Alignment

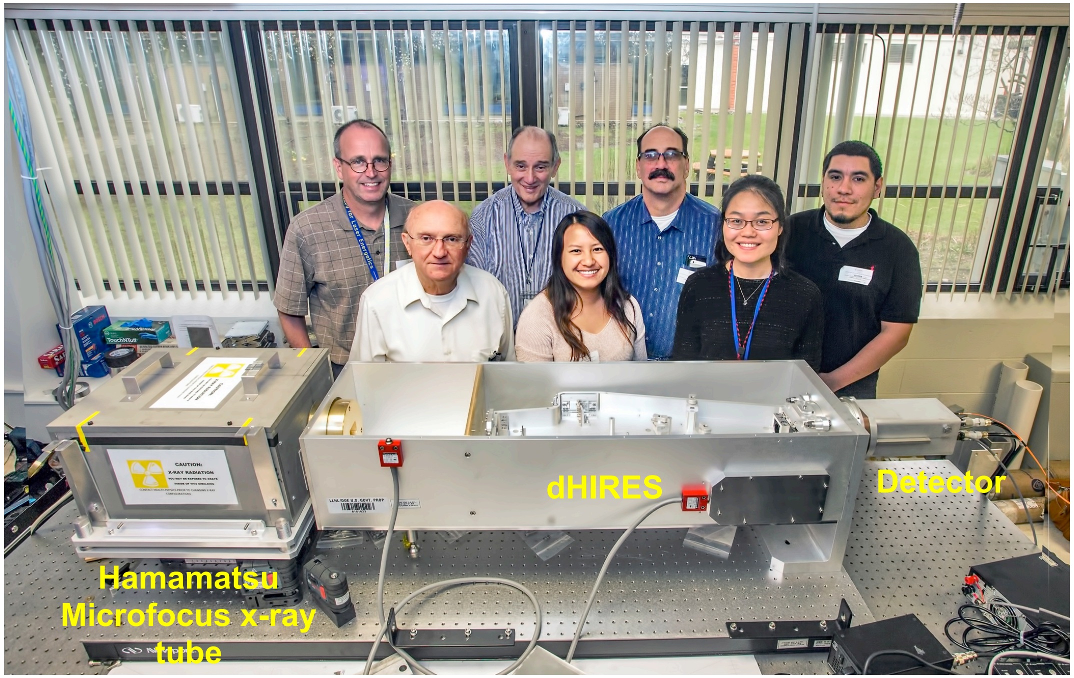

The spectral resolution is ~10 eV

*L. Gao et al, RSI invited, accepted

Stark broadening of Kr Heβ measures n_e and ratio of He-like resonance line to Li-like satellite provides T_e

SCRAM calculation for a SymCap implosion
Cr: D. Liedahl

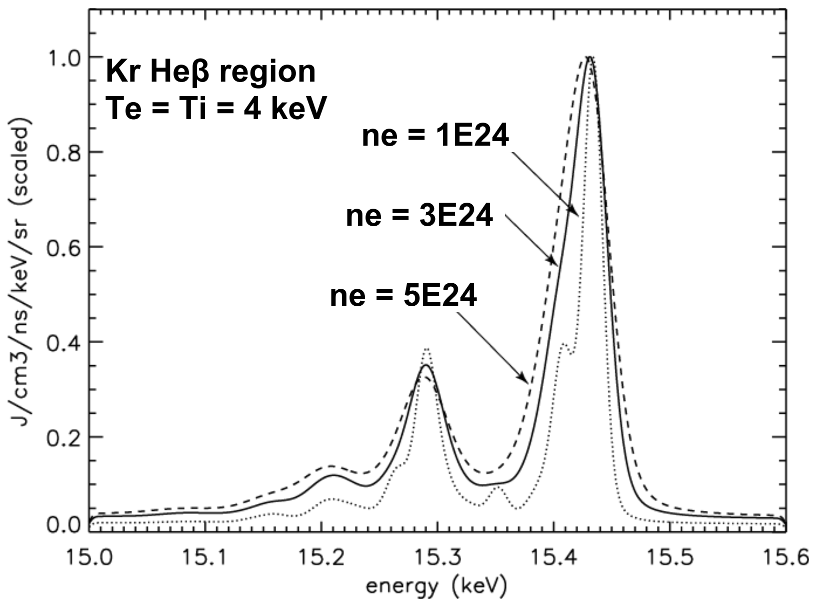

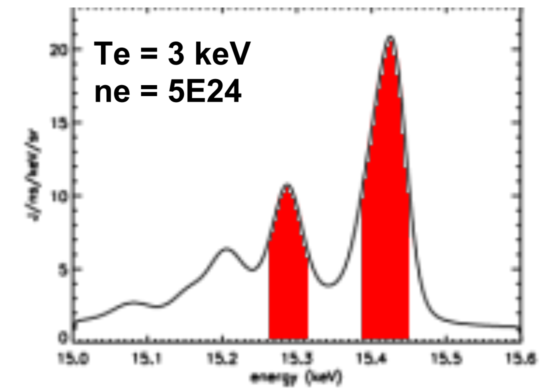

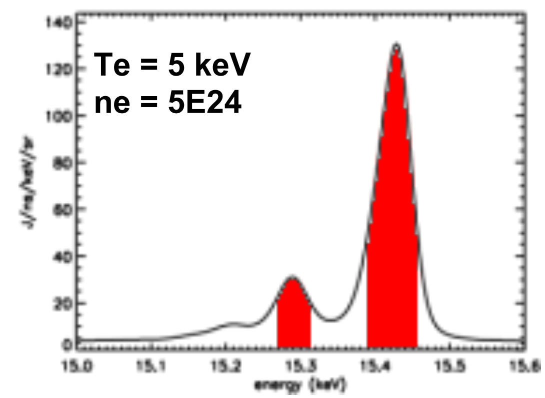

First DHIRES data was collected from a Polar Direct-drive Exploding Pusher (PDXP) experiment* N170928-001-999

192 Beams
0.5 MJ, 1.8 ns

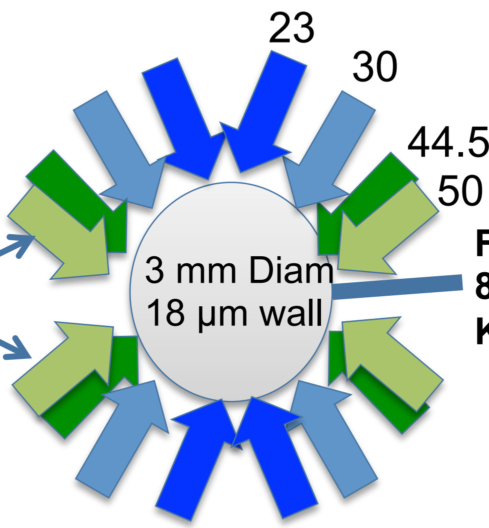

Fill tube
8 atm D_2
Kr at 0.005 at.%

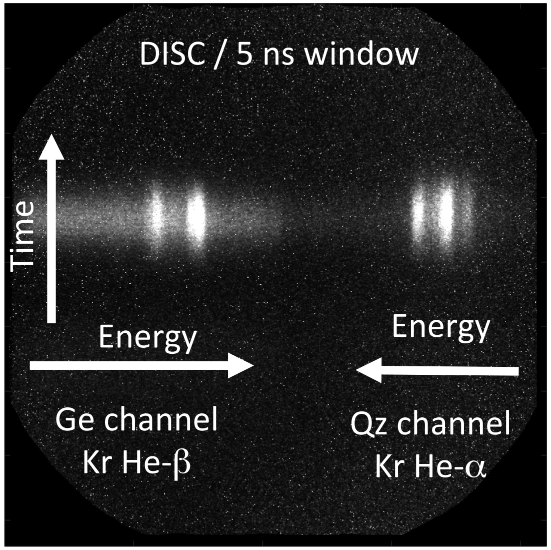

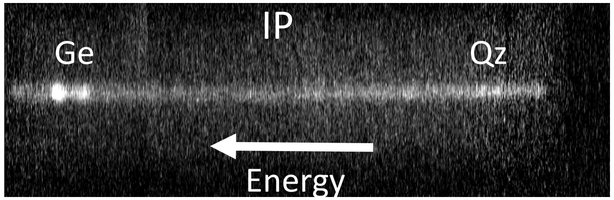

*H. Whitley, PDXP team

Ratio of resonance peak to satellite peak will yield a measure of $T_e(t)$

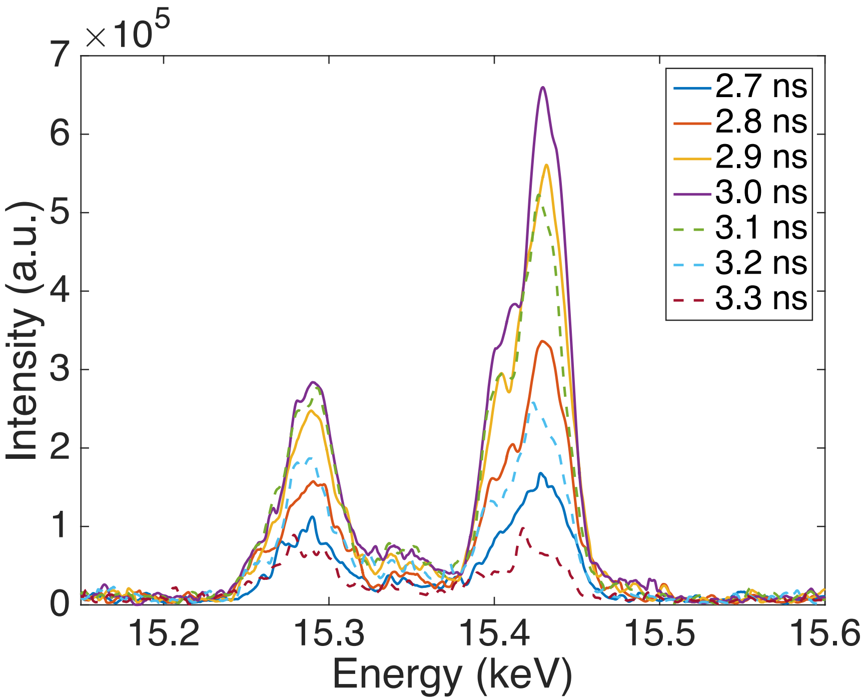

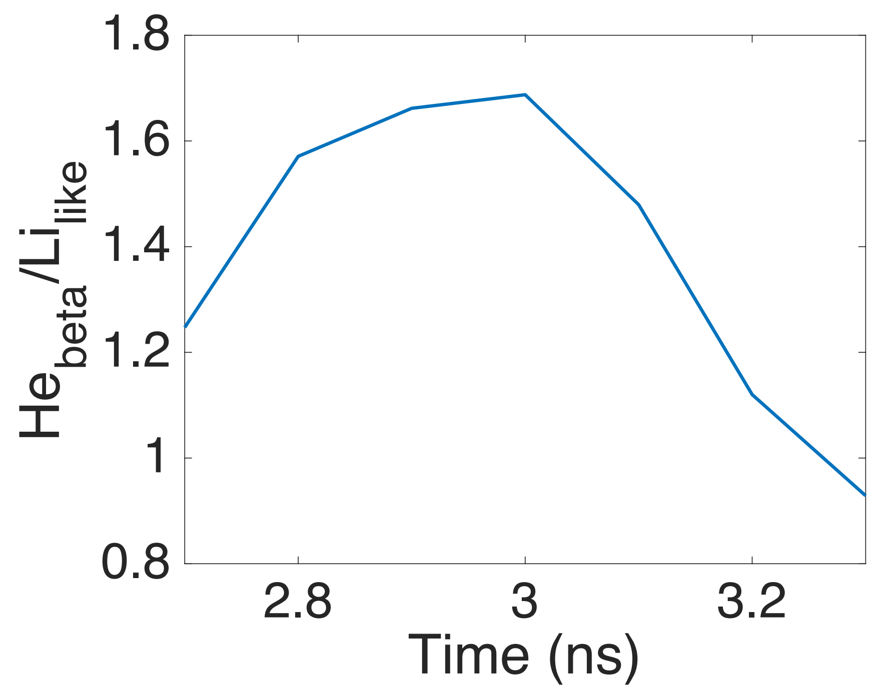

The time-integrated channel will be used to cross calibrate the two streaked channels

Reconstructed source emission from IP data

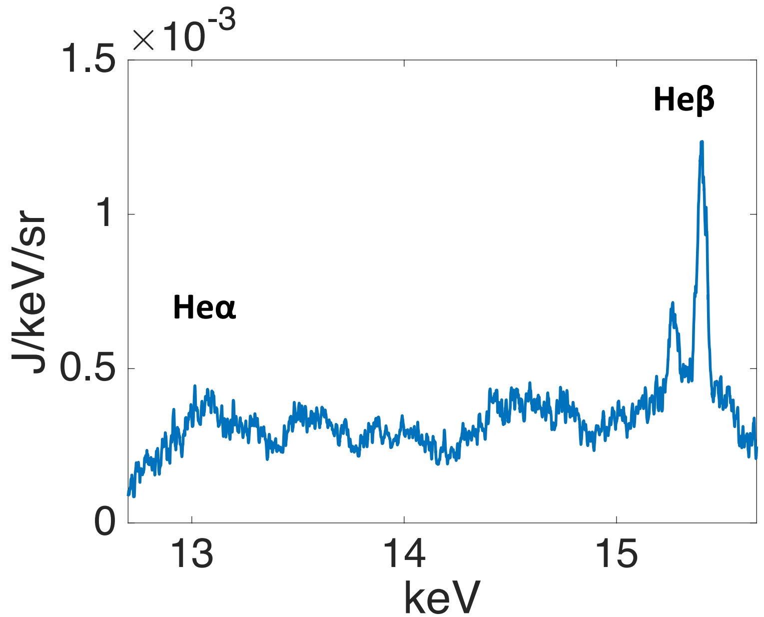

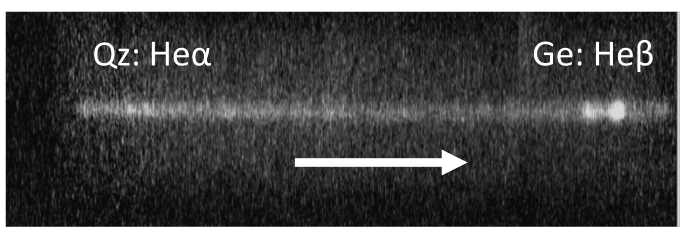

X-ray radiography, coupled with x-ray framing camera, is used to radiograph instability growth

- The backlighter transmission depends on wavelength and target optical depth; mass perturbations lead to optical-depth perturbations

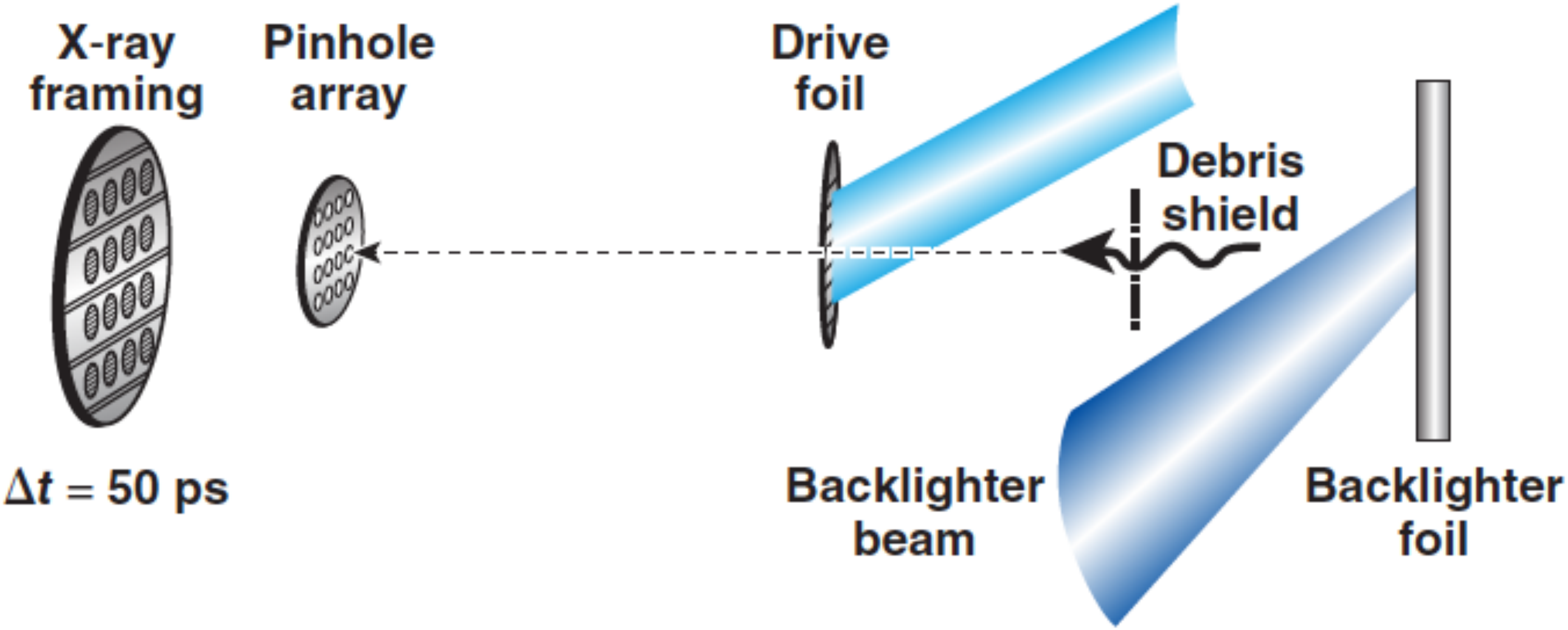

	Framing cameras
Spatial resolution	8 to 10 μm (two dimensions)
Spatial field of view	500 μm (magnification = 12)
Temporal resolution	30 to 80 ps
Temporal field	(four) 300-ps strips

A bubble merger is predicted in the nonlinear phase of the RT instability*

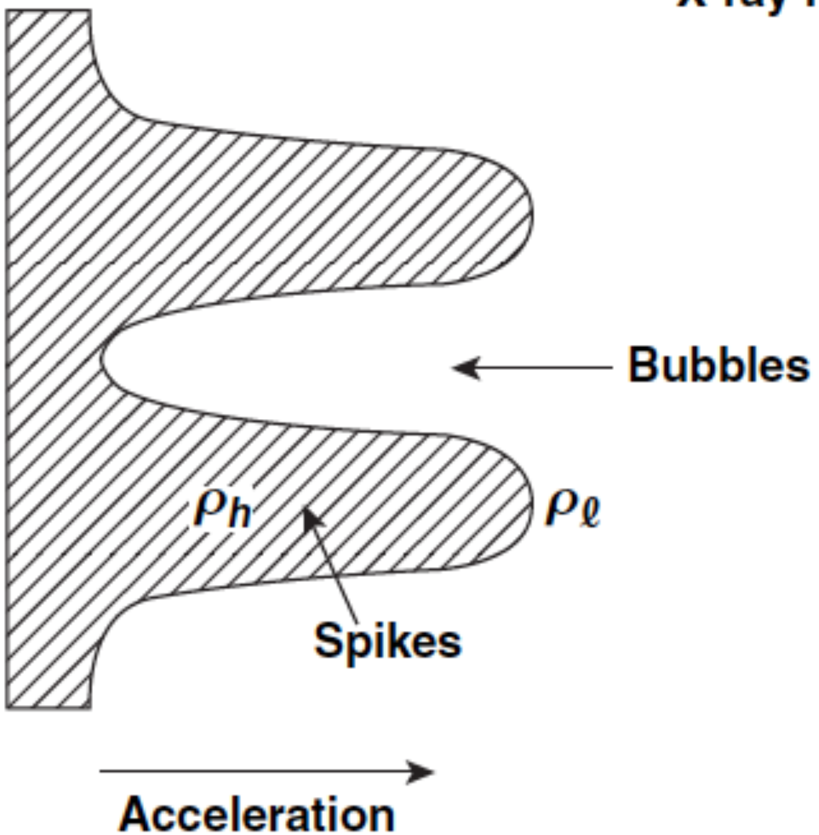

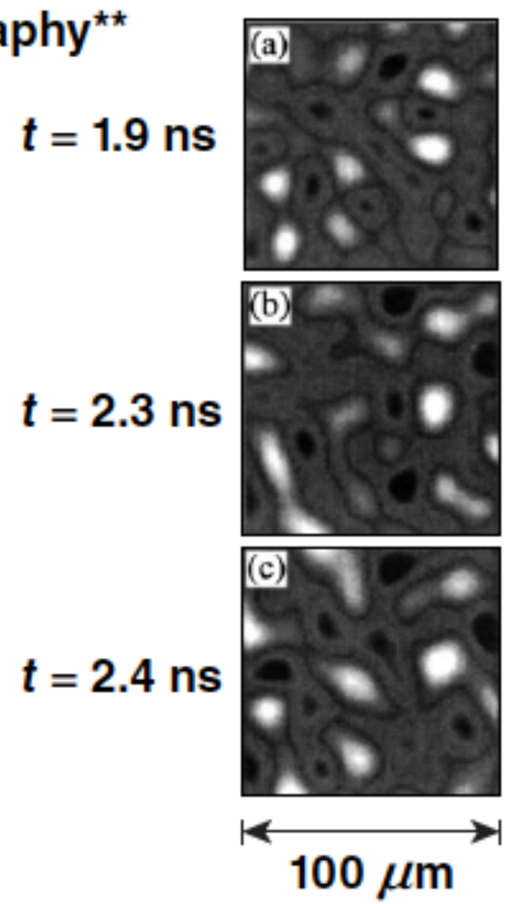

X-ray photons are sensitive to density modulations.

*D. Oron *et al.*, Phys. Plasmas 8, 2883 (2001);
U. Alon *et al.*, Phys. Rev. Lett. 72, 2867 (1994).
**V. A. Smalyuk *et al.*, Phys. Rev. Lett. 81, 5342 (1998).

Optical Thomson scattering is used to diagnose local plasma conditions by observing the spectrum of light scattered from a probe beam over a small interaction volume

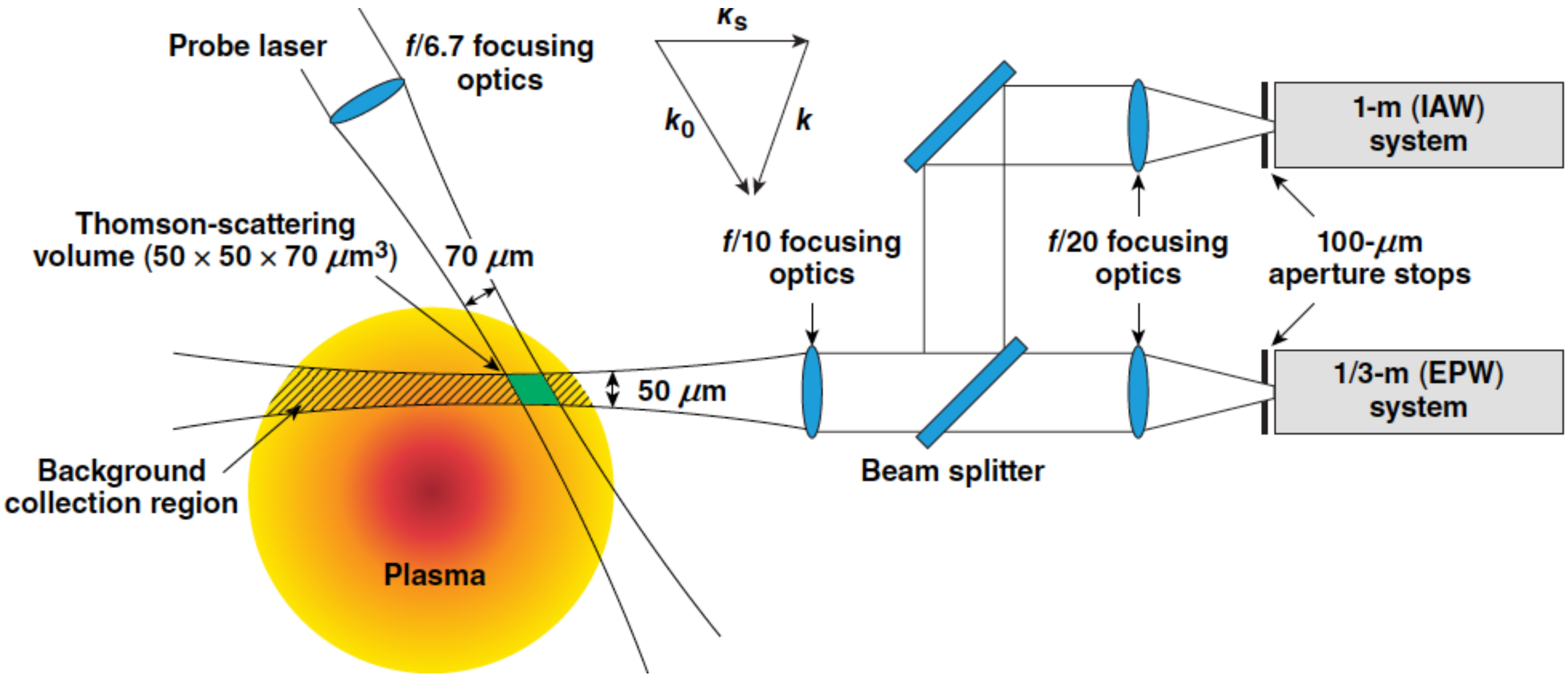

*R. Follet et al, RSI 87, 11E401 (2016)

Plasma parameters are inferred by comparing measured Thomson-scattering spectra to calculated spectra

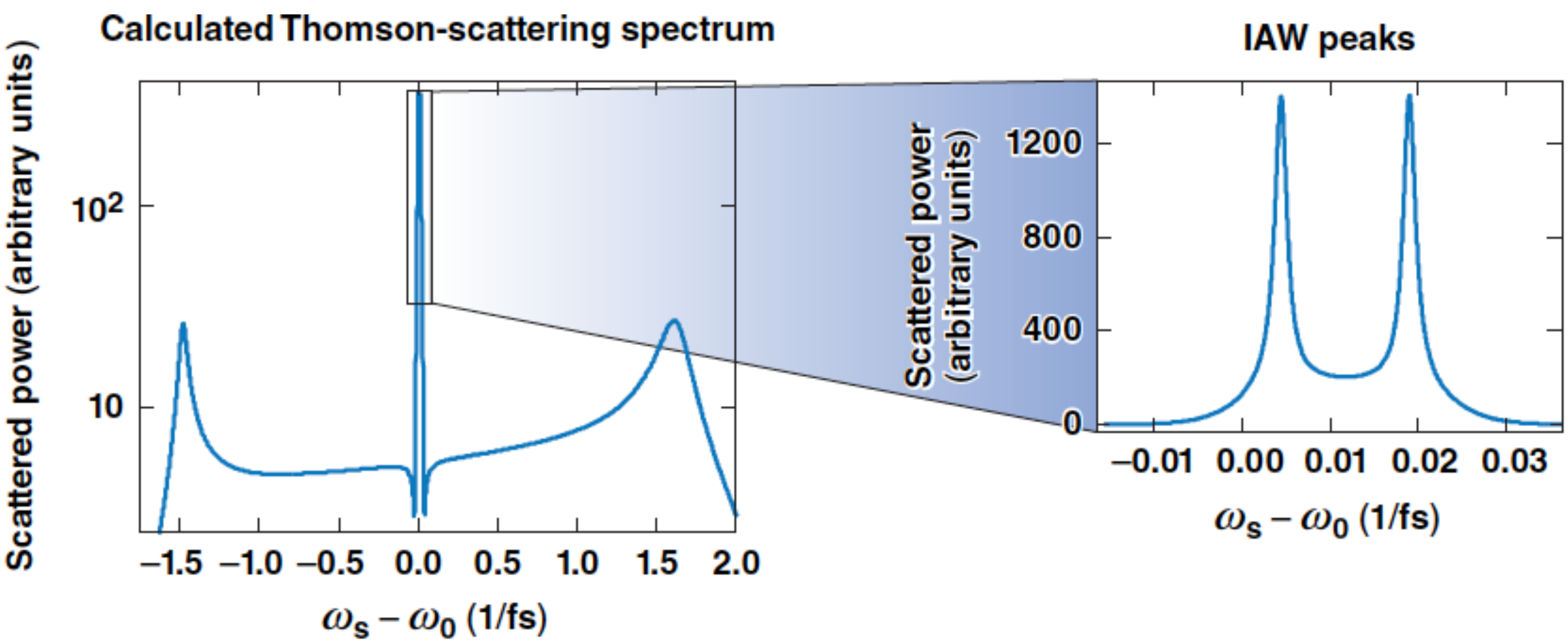

Approximate frequency shift for scattering from

EPW's: $\Delta\omega_\pm = (\omega_s - \omega_0) = \pm\sqrt{\omega_{pe}^2 + 3k^2 v_{te}^2}$

IAW's: $\Delta\omega_\pm = (\omega_s - \omega_0) = \pm k c_s - \vec{k} \cdot \vec{u}$

*R. Follet et al, RSI 87, 11E401 (2016)

Electron density and temperature, ion temperature, and flow velocity were measured inside the magnetized jet

OMEGA beams:
- Ring 1: 17, 22, 46, 56, 61
- Ring 2: 11, 26, 31, 55, 68
- Ring 3: 10, 13, 20, 28, 33, 48, 52, 58, 65, 66

OMEGA EP BL:
- Maximum energy, 10 ps (may switch to 1 ps)
- Best focus
- 8 mm from TCC toward H7

Diagnostics:
- TIM 5: Titled CPRM as the proton detector
  Distance is 16.5 cm from TCC
- TIM 6: TS collection system
- TIM 3: TTPS for the main plastic target
- **TIM 4: XRFC (changed from TIM 2 to TIM 4)**
- H2: EP proton generation assembly target stalk

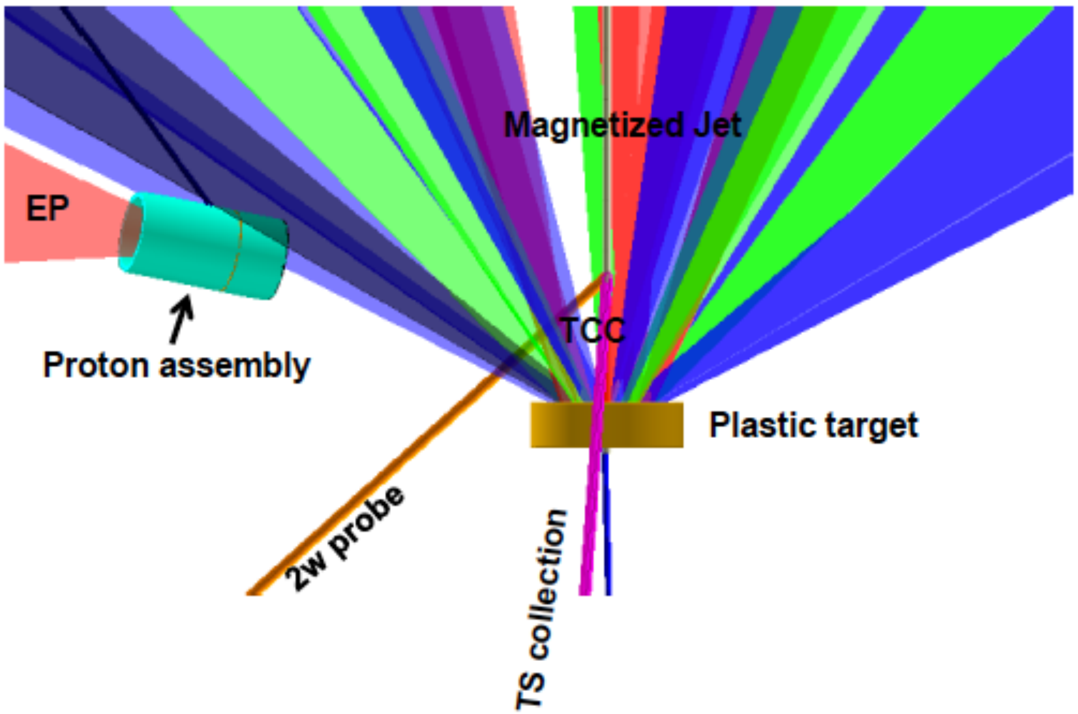

Electron density and temperature, ion temperature, and flow velocity were measured inside the magnetized jet

EPW feature (d=400 μm)

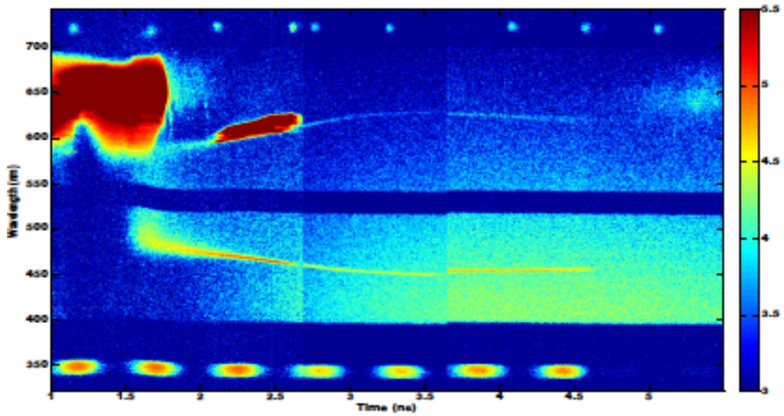

IAW feature (d=400 μm)

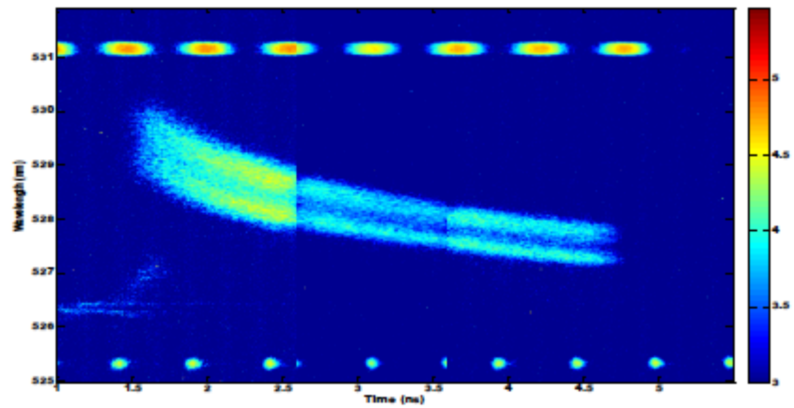

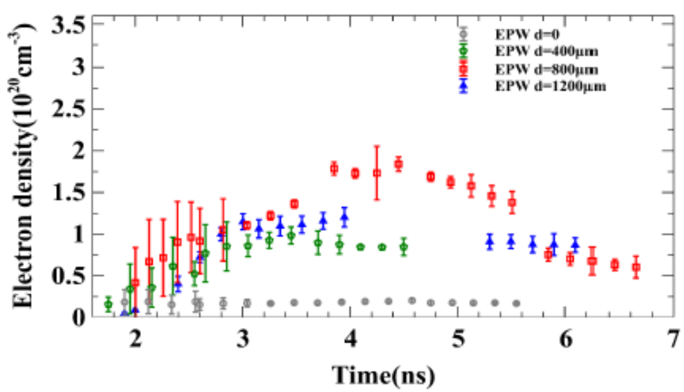

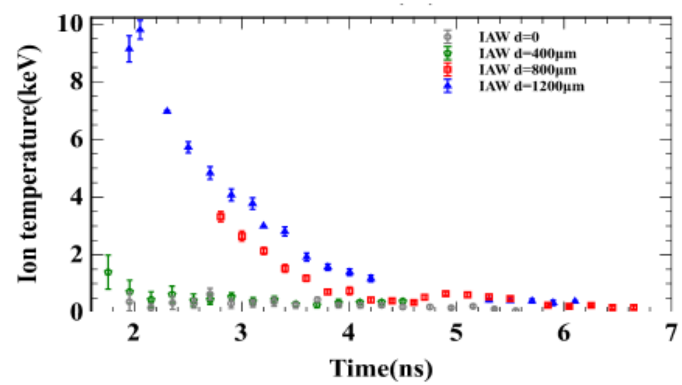

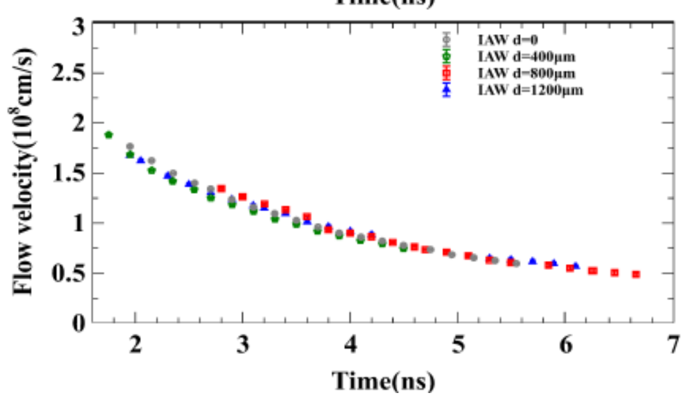

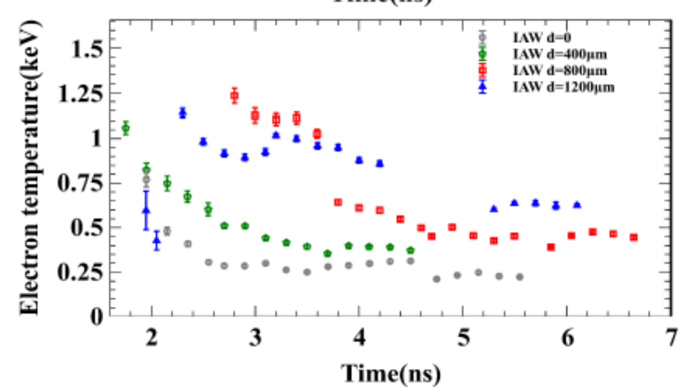

The neutron spectrum provides information on ρR, Ti and yield – essential for assessing the implosion performance

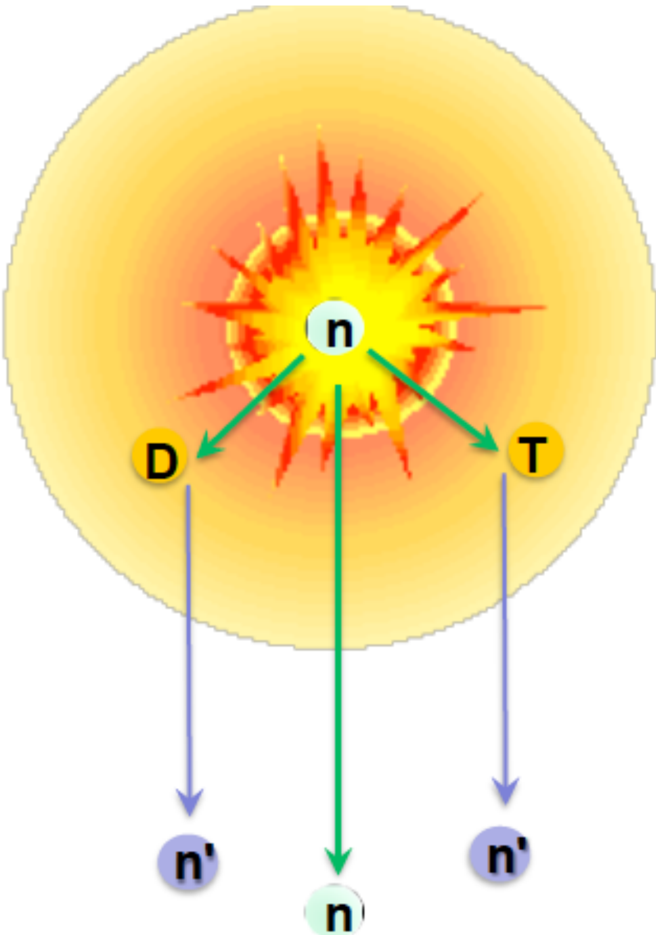

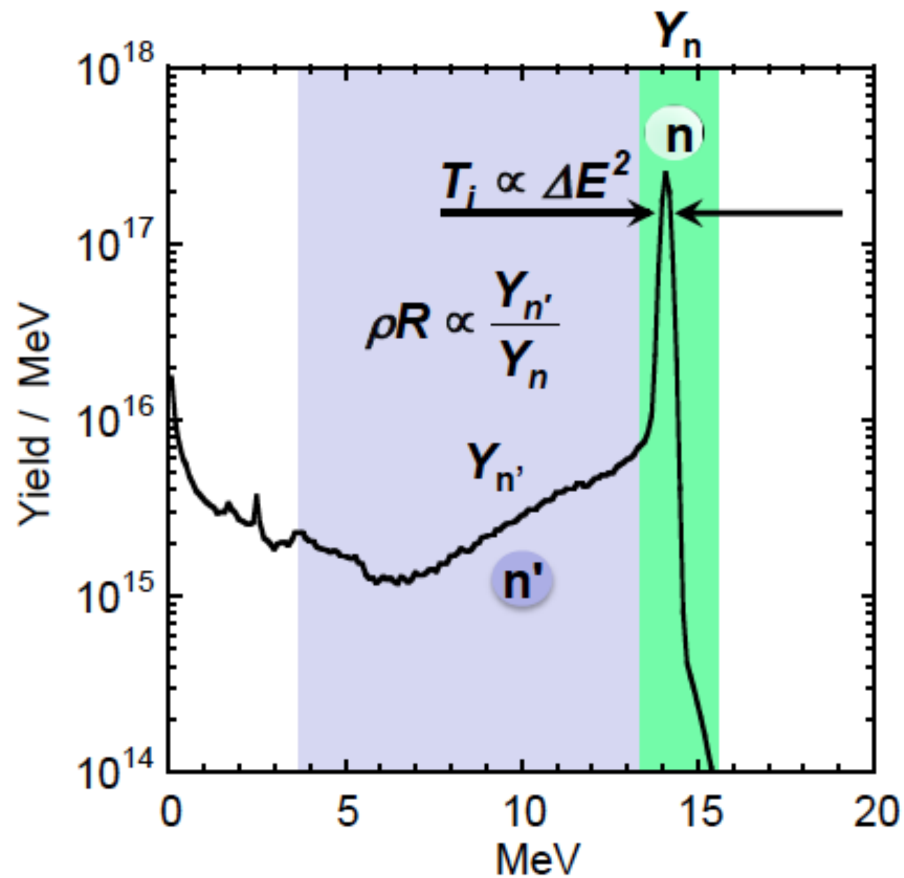

A large suite of diagnostics have been developed for HEDP facilities

- HEDP systems generate some or all of
  - Visible light
  - UV and x-ray photons
  - Charged particles
  - Neutrons
  - Strong fields
- A comprehensive diagnostic suite makes it possible to learn a great deal about the systems: field strength and their impact, plasma parameters (n_e, n_i, T_e, v), particles, instabilities, yield, etc…
- Diagnosing HED systems require very high temporal (sub-ns, ps) and spatial (~10 μm) resolution
- Advances in technology and diagnostics enable understanding of new physics